Sustainable Energy Technologies and Assessments 89 (2026) 105000

Contents lists available at ScienceDirect

Sustainable Energy Technologies and Assessments

journal homepage: www.elsevier.com/locate/seta

Decarbonization of industries using reverse brayton high temperature heat pumps: A case study in the ceramic industry

Dimitrios N. Korres [a], Evangelos Bellos [a,b], Nikolaos Nikolopoulos [a,*], Varshil Dalal [c], Panagiotis Stathopoulos [c], Apostolos Gkountas [d], Pantelis Bakalis [d], Ilias K. Tragazikis [e], Agis Kothalis [e]

[a] *Chemical Process & Energy Resources Institute, Centre of Research and Technology Hellas, Marousi, Egialeias 52, Athens 15125, Attica, Greece*
[b] *Department of Mechanical Engineering, School of Engineering, University of West Attica, 250 Thivon & Petrou Ralli, Athens 12244, Greece*
[c] *Institute of Low-Carbon Industrial Processes, German Aerospace Center (DLR), Cottbus, Germany*
[d] *Psyctotherm SME, Piraeus 18540, Greece*
[e] *KEBE SA, Nea Santa, Kilkis 61100, Greece*

ARTICLE INFO

Keywords:
Reverse brayton HTHP
Ceramics industry
Optimization analysis
Dynamic analysis
Environmental impact
Energy savings

ABSTRACT

A closed-loop Reverse-Brayton High Temperature Heat Pump with air working medium is studied and optimized considering real operating conditions for a ceramic industry. The heat pump was considered to upgrade the waste heat of the kiln's exhaust gases into useful heat for further heating up the combustion air. All the necessary thermodynamic variables are determined by calculating the compressor and turbine work, the input power, the coefficient of performance, and the exergy efficiency. First, a detailed optimization procedure is carried out for various inlet preheated air temperatures in the range of 100–200 °C, with the primary aim being the maximization of the heat pump performance (COP maximization) by identifying the optimal working-medium mass flow rate for each preheated air temperature level. Secondly, for the defined optimized operating conditions, a dynamic analysis was performed for a typical week of operation, considering real data with inlet preheated air temperatures within the range of 106.8–179 °C (typical week fluctuation) and considering operation under optimized mass flow rate values. It was found that the integration of HTHP leads to 1.36% primary energy savings and 5.44% CO_2 emissions reduction on a yearly basis, ensuring a slightly lower annual operating cost than the respective of natural gas combustion.

Introduction

The increasing need for energy efficiency and for the reduction of greenhouse gas emissions, especially in high-scale industrial production lines, is a crucial aspect of the contemporary energy-intensive industries, which embody technologies for high-temperature level heat production [1]. These industries have huge energy demands and they are accompanied by significant amounts of waste heat, in temperatures within 100–200 °C, coming from the high-temperature heating processes that take place within the production procedures [2,3]. This has led to significant interest in waste heat recovery regarding energy-intensive industrial systems.

Among the industries in which waste heat recovery can make a notable impact, ceramics production stands out, due to its energy-intensive nature and reliance on high-temperature processes. In study [4], it was reported that the global market of the ceramics sector counts $229.13 billion estimated value, with the overall ceramics production, including roof tiles and bricks, responsible for the emission of a total 19 Mt_{CO2eq}/year in the EU [5]. The ceramic industry seems to be one of the best representatives of the energy-intensive industries, since high-temperature heat is needed in the majority of the processes involved, especially considering the production of ceramic roof tiles and bricks [5]. The energy needs of a ceramic industry could extend from some kWh up to more than 200 MWh_{th} on a daily basis, considering a continuous operation (24/7) in most cases. The main thermal processes that take place in a ceramic industry are drying, preheating, combustion and cooling process [4], considering a tunnel type kiln in most cases [6]. The temperature ranges are 80–150 °C [7], 200–600 °C, 900–1100 °C and 80–150 °C respectively [8–10]. The processed material, first, passes through the dryer and the humidity of the raw material drops approximately to zero, with the contained water to be released to the

* Corresponding author.
E-mail address: n.nikolopoulos@certh.gr (N. Nikolopoulos).

https://doi.org/10.1016/j.seta.2026.105000
Received 23 January 2026; Received in revised form 3 April 2026; Accepted 25 April 2026
Available online 29 April 2026

Nomenclature

C	Total heat capacity, W/K
COP	Coefficient of Performance
Cp	Specific heat capacity, J/(kg K)
Dp	Pressure drop, Pa
eff	Effectiveness
Ex	Exergy rate, W
h	Specific enthalpy, J/kg
$\dot{m}$	Mass flow rate, kg/s
P	Power, W
p	pressure, Pa
PR	Pressure ratio
$\dot{Q}$	Thermal power, W
T	Temperature, K
$\dot{W}$	Work, W

Greek symbols

η	Efficiency

Subscripts

1	Point 1 of the cycle
2	Point 2 of the cycle
3a	Point 3a of the cycle
3b	Point 3b of the cycle
4	Point 4 of the cycle
5	Point 5 of the cycle
C	Compressor
EG	Exhaust gases
el	Electrical
elm	Electromechanical
high	High pressure
HTHE	High Temperature Heat Exchanger
in	Inlet (for T), Input (for Q)
is	Isentropic
low	Low pressure
LTHE	Low Temperature Heat Exchanger
max	Maximum
min	Minimum
motor	Motor
NG	Natural Gas
out	Outlet (for T), Output (for Q)
opt	Optimum
PA	Preheated Air
R	HTHP working medium
ref	Reference
REC	Recuperator
T	Turbine

Abbreviations

HTHE	High Temperature Heat Exchanger
HTHP	High Temperature Heat Pump
LTHE	Low Temperature Heat Exchanger
NG	Natural Gas
REC	Recuperator

environment in the form of vapor. Then, the processed material is preheated and directed to the combustion zone, where the maximum heat is obtained to achieve the desired properties. Afterwards, the processed material is cooled down and becomes the final product ready for the packaging process [4]. In most ceramic industries, the major heat demand in the combustion zone is covered by natural gas (NG) or fuel oil combustion engines [11]. The exhaust gases are often utilized or recovered for the drying or the preheating phase or even for preheating the combustion air by ensuring up to 30% cost savings for the industry [12,13]. Although the aforementioned heat recovery offers important energy savings, the exhaust gases still leave the kiln in relatively high temperatures within the range of 70–100 °C as waste heat, which cannot be further utilized in any of the kiln's processes. Hence, great emphasis should be given to the recovery of the aforementioned waste heat through new technologies aiming at the reduction of energy/fuel consumption. The use of High Temperature Heat Pumps (HTHPs) has emerged as a promising solution to recover and reuse industrial waste heat of relatively low grade (50–100 °C) and upgrade it into high temperature useful heat [3], for preheating the combustion air of the natural gas burners, which are used in the firing section of the kiln in most cases. A remarkable interest has been observed over recent years as regards the implementation of HTHPs in industrial sites for waste heat upgrade with potential energy savings of up to 30% [3] and capability of covering over 70% of the process heat needed in temperatures up to 150 °C, ensuring at the same a total process heat demand coverage of around 40% [11].

Extended research has been conducted regarding the integration of HTHPs in industrial processes for waste heat upgrade, reaching temperatures of up to 100–150 °C with available heat source temperature levels of 50–60 °C and heat sink temperatures around 100 °C [14,15]. Deng et al. [16] examined the operation of a novel high temperature heat pump experimentally, considering a 50 °C heat source and found that a 130 °C heat sink could be obtained, ensuring a COP of 2.74. A single-stage HTHP is tested in the study [17] and it was revealed that a heat sink in the range of 80–110 °C was achieved for an input heat source near 50–70 °C. A cascade high-temperature heat pump is proposed by Dong et al. [18]. It was found that the examined heat pump could ensure a temperature lift of approximately 90 °C from 30 °C to 120 °C and from 5 °C to 90 °C with COP values around 2.2. Great emphasis has been given to the mechanical compression closed-circuit HTHPs since this type is available in a wide operating range and it appears in most industrial applications [19]. However, there is a lack in existing scientific literature as regards HTHP systems that ensure high temperatures greater than 100–150 °C and especially up to at least 200 °C, due to the fact that such temperatures are hard to obtain by conventional HTHPs [19].

This difficulty seems to be overcome with the utilization of closed-loop Reverse Brayton cycle HTHPs, which could serve relatively high temperature applications even in the range of 250–300 °C by taking advantage of relatively low temperature heat sources of 50–100 °C, according to recent studies [20]. The aforementioned heat sink temperatures are mainly met in energy-intensive industries in the ceramics sector and thus, the Reverse Brayton cycle HTHP technology constitutes a promising solution for this industrial sector. Numerous scientific studies focus on the exploitation of the industrial waste heat with the integration of Reverse Brayton cycle HTHPs have been conducted. Kabat et al. [21] investigated a Reverse Brayton cycle heat pump aiming to optimize the performance considering a heat sink temperature near 250 °C with the respective heat source one to be within −30 °C to 5 °C. They found that a COP in the range of 2.0–2.3 was obtained. The same researchers also conducted a study [22] in which they compared the simple Reverse Brayton cycle to a complex one with an intercooler and recuperator, considering heat upgrade from −30 °C (process cooling) to 250 °C (process heating) and they found that the performance of the complex cycle exceeds the simple one by approximately 6%. Yucel et al. [23] experimentally analyzed the operation of a two-stage HTHP following the Reverse Brayton cycle and they reported that the heat sink temperature could reach 205 °C with a heat source of −10 °C. Tzouganakis et al. [24] proposed a novel solar-driven Reverse Brayton HTHP for process heat production in a paper mill industry for upgrading process air from 150 °C to 195 °C, ensuring a mean COP around 1.5. Another similar setup in the food industry was examined by the same researchers [25]. The scope of that research work was to upgrade 245 °C process air to 255 °C with the utilization of solar collectors and waste heat coming from flue gas. The COP in that case was calculated to slightly exceed 1.5. Pettinari et al. [26] conducted a transient analysis of an HTHP to investigate its operation during cold start-up and found that the heat exchangers' design plays an important role in the start-up time, since the last one is reduced by more than 50%. Several novel combined cycles with thermally coupled micro gas turbines (MGTs) and HTHPs are presented in the study of Ref. [27] and it was found that such combinations could lead to a significant reduction of the HTHP energy consumption.

The existing literature places considerable emphasis on industrial high-temperature heat pumps (HTHPs). However, to the best of the authors' knowledge, very limited scientific research has been conducted on waste heat recovery applications involving HTHP integration in the ceramics sector, despite the fact that ceramics production represents a significant industrial market. Following an in-depth review of the available literature, only one recent scientific publication (Ref. [5]) was identified that investigates the integration of HTHPs for waste heat recovery in the ceramics industry. Reference [5] presents a noteworthy study that examines a conventional HTHP configuration for a hypothetical ceramic tile production facility. The analysis is conducted under steady-state conditions, assuming a single preheated air inlet temperature of 70 °C and a constant mass flow rate of 5.3 kg/s, while suggesting multi-objective optimization as a direction for future work. In contrast, the present study is the first in the literature to investigate a single-stage Reverse Brayton cycle HTHP for integration into a real industrial site in the ceramics sector. The analysis combines steady-state multi-objective optimization with a dynamic performance assessment based on real operating data obtained from an existing ceramic production facility. Another important contribution of the present work is that the dynamic analysis is performed by determining the optimal working-fluid mass flow rate at each operating point, ensuring maximum coefficient of performance (COP) throughout the examined operating period.

Table 1 summarizes the main novelties of the present work in comparison with the existing study reported in Ref. [5] regarding waste heat recovery using HTHPs in the ceramics industry. The comparison focuses primarily on the HTHP technology employed, the type of analysis performed, the optimization strategy adopted, and the model verification approach.

In particular, a closed-loop reverse Brayton HTHP with recuperator and air as a working medium is examined in detail in this study, considering its integration in the ceramics industry of KEBE [28] located in northern Greece. The available real industrial input data, which is being utilized in this work, gives the opportunity to estimate the sustainability benefits and the energy saving achieved by the proposed HTHP. More specifically, HTHP performance is optimized (in terms of achievable COP) under specific operating conditions while its dynamic operation is investigated considering real operating data taken directly from the industry. The examined HTHP is proposed to upgrade the 90 °C waste heat (exhaust gases) to around 200 °C to further heat the preheated air, supplied to the kiln for NG combustion, aiming at the reduction of energy consumption in the combustion zone. A detailed optimization procedure takes place, first, for inlet preheated air temperatures within 100–200 °C, focusing on the maximization of COP through the determination of the optimum working medium mass flow rate for each temperature. Next, the operation of HTHP is evaluated via a thorough dynamic investigation for a typical week (total period of 168 h), since a 24/7 operation is considered. The optimal mass flow rate values from the optimization process are adopted here to ensure optimum dynamic operation of the HTHP. The main parameters that are calculated are all the thermodynamic state properties within the cycle and the heat exchangers' secondary circuits, the work of the turbine and the compressor, the electrical power for the compressor's motor, the input power coming from the waste heat source, the COP and the exergy efficiency of the system. Annual energy savings and the CO_2 emissions reduction are also calculated and compared against the case without the HTHP. Both the optimization and the dynamic analysis models are developed in MATLAB. The parametric optimization model is verified by an equivalent model developed in EBSILON software, showing small deviations (<0.6%).

Materials and methods

The examined industrial case study

In the present work, a High-Temperature Heat Pump (HTHP) was studied for its design, dimensioning and deployment at the industrial environment of the KEBE ceramic industry unit located in Northern Greece (Nea Santa, Kilkis, 40.84° N and 22.82° E), as part of the European Horizon project EEETHOS [29]. The operation of the particular industrial unit runs 24/7, excluding some specific periods during the year when the unit is set out of operation for maintenance purposes. This industrial site is divided into two main production lines, i.e., i) the roof tiles and ii) the bricks production lines. This work focuses on the roof-tile production line, and specifically on the tunnel kiln, where the HTHP is planned to be installed. The roof tile production line is capable of producing large amounts of several different types of tiles, with an average production volume reaching even 160,000 pieces per day. The operation of the kiln in the roof tile section is considered to be almost steady with no significant ups and downs, considering that the fluctuation of the production volume (tonnage) entering the kiln is very small compared to the large capacity of the kiln. The existing process, as of today, utilizes a natural gas (NG) based system with gas burners for achieving the desired temperatures inside the tunnel kiln. The last one is separated into three main zones: i) preheating (from 25 °C to 700 °C), ii) combustion (up to 960 °C) and iii) cooling zone (from 960 °C down to 30 °C). The tiles leaving the dryer chamber enter the kiln's preheating zone, where they are heated to about 700 °C using the relatively high thermal level of the exhaust gases. In the subsequent main combustion zone, the tiles are heated at the maximum possible rate, while in the cooling zone, they are cooled using ambient air. This cooling air is then directed to the combustion zone, where it is used as combustion air. A detailed view of the roof tiles production line is depicted in Fig. 1.

The main concept of the proposed decarbonization measure examined in this study is the introduction of an electrification-based process that exploits and upgrades the heat of the preheated air exiting the

Table 1
Comparison of the present work with the study in Ref. [5].

Study	Technology	Analysis type	Optimization	Pressure Losses	Input data	Model Verification
Ref. [5]	Classic HTHP	Steady state	NO	2% assumption	One hypothetical operating point (70 °C)	NO
Present study	Reverse Brayton HTHP	Steady state & Dynamic	YES (multi-objective) - Determination of the optimum mass flow rate in each operating point.	Calculated via UNILAB software	Steady state analysis: Numerous operating points (100–200 °C) & Dynamic analysis: Real data from industry (168 h of operation)	YES (via EBSILON software)

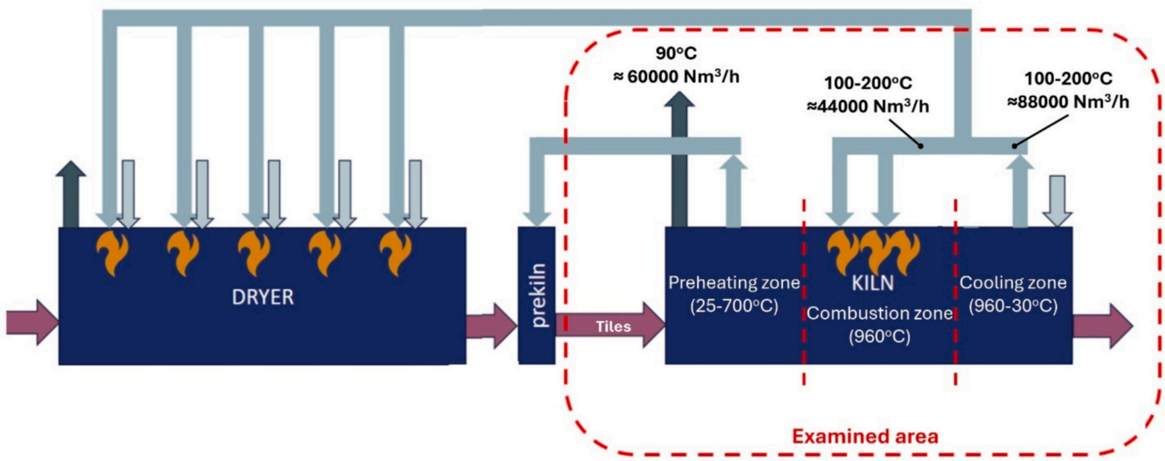

Fig. 1. Rooftiles production line in KEBE industrial unit in Nea Santa-Kilkis, Greece.

cooling zone, thereby providing warmer combustion air to the burners, reducing natural gas consumption, while ensuring the highest possible energy savings. The most suitable solution for meeting the heat-upgrade and energy-saving requirements in the KEBE roof-tile production line was the integration of an HTHP. This HTHP operates on a closed-loop Reverse Brayton cycle using air as the working medium. The system works by recovering and upgrading the waste heat contained within the exhaust gases from the preheating zone, subsequently using that energy to further heat the preheated combustion air.

Considering that the new integrated HTHP thermal capacity was selected to be 1 MW_{th}, and operation of the production line is almost 24 h daily, the thermal energy provided to the industry is calculated at 24 MWh_{th}/day. Considering that the KEBE's roof-tile production line typically requires 230 MWh_{th} of natural gas per day (approximately 180–200 MWh_{th} thermal energy), the introduction of the HTHP unit, as examined in this study, can provide more than 10% of the total thermal energy demand, highlighting its significant contribution to the process.

The examined high temperature heat pump

HTHPs designed for systems operating at up to 300 °C cannot utilize conventional refrigeration equipment, such as reciprocating or screw compressors, which are limited by the thermal constraints of standard refrigerants and lubricants. Instead, these advanced HTHP systems often employ robust, high-performance components adapted from demanding industries. Specifically, equipment originating from the automotive industry, such as turbochargers (which inherently handle high temperatures and pressure ratios), are modified and employed as efficient compressors or expanders to manage the extreme operating conditions and high temperatures required for industrial waste heat recovery. The

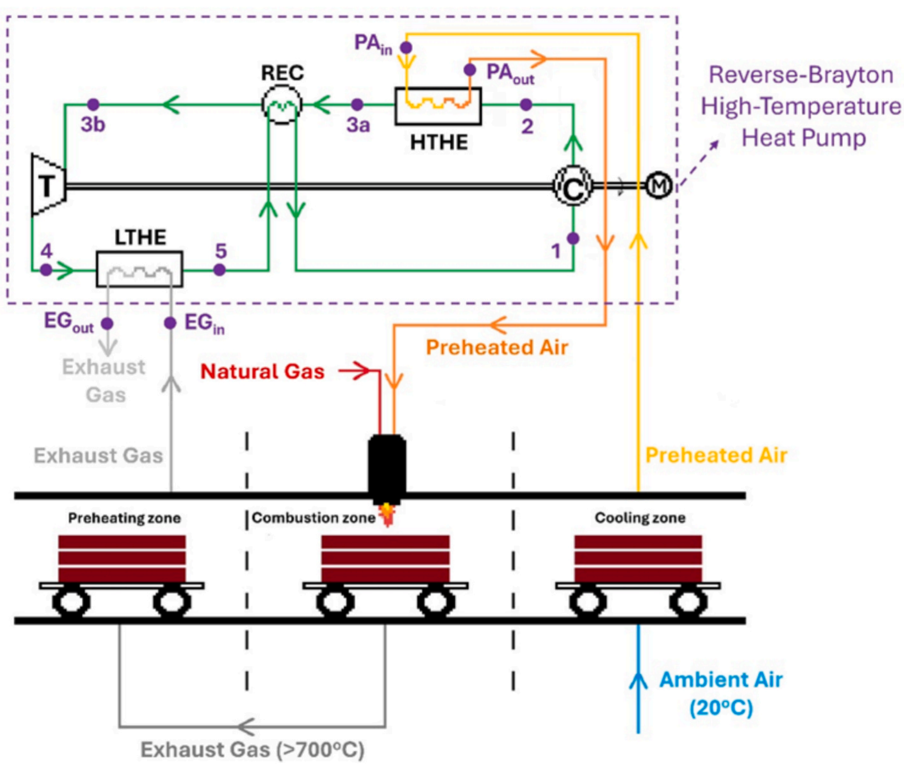

Fig. 2. Schematic diagram of the process with the integrated HTHP.

design of the specific HTHP is based on a reversed closed Brayton cycle, which involves as main components a Low Temperature Heat Exchanger (LTHE), a High Temperature Heat Exchanger (HTHE), a Recuperator (REC) and a turbo-compressor unit for the compression and the expansion of the working medium. A schematic depiction of the initial design consideration is provided in Fig. 2, presenting the main operating principle of the HTHP and clarifying its integration into the existing setup in the ceramic industry. As shown in Fig. 2, the exhaust gases from the combustion zone enter the preheating zone to preheat the roof tiles. Subsequently, instead of being released directly to the environment as in the baseline scenario, these gases are directed to the LTHE of the integrated HTHP. Within the LTHE, the HTHP's closed-circuit air recovers heat from the exhaust gases (state 4), while the air is then directed to the recuperator for further heating (state 5). After exiting the recuperator at a low-pressure stage, the air is compressed by the compressor of the turbo-charger unit, upgrading it to the high-pressure and high-temperature conditions of the Reverse Brayton cycle (state 2). Next, the compressed air is cooled by passing through the HTHE, where heat is conveyed to the combustion (preheated) air in the secondary circuit of the HTHE (state 3a). Following this, the working air flows to the recuperator's primary circuit to transfer heat from the high-pressure to the low-pressure stage (recuperator secondary circuit) after the LTHE (state 3b). Finally, the high-pressure air is expanded in the turbine (state 4) of the turbo-charger unit, generating mechanical work, which serves as an auxiliary input to the compressor, considering that the turbine and the compressor are connected with the same shaft.

The thermodynamic cycle of the Reverse Brayton HTHP stands alone in Fig. 3a for explaining the temperature regime in the inlet and the outlet of the two main heat exchangers of the HTHP (LTHE and HTHE) qualitatively, while the Temperature – specific entropy diagram (T-s) is provided in Fig. 3b for getting an overview of the thermodynamic behavior of the cycle. It should be mentioned that the T-s diagram was created considering a typical case based on the operating conditions presented in section 2.3.

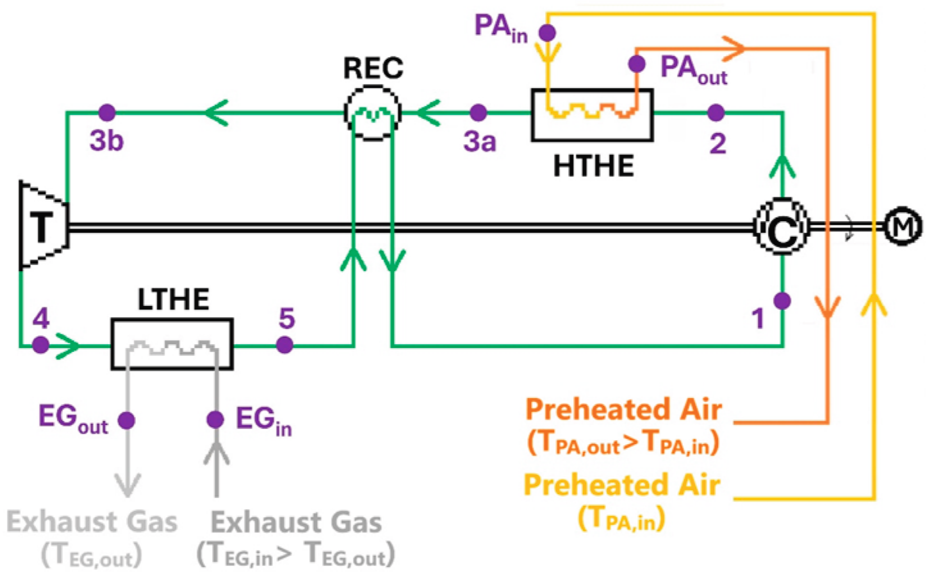

(a)

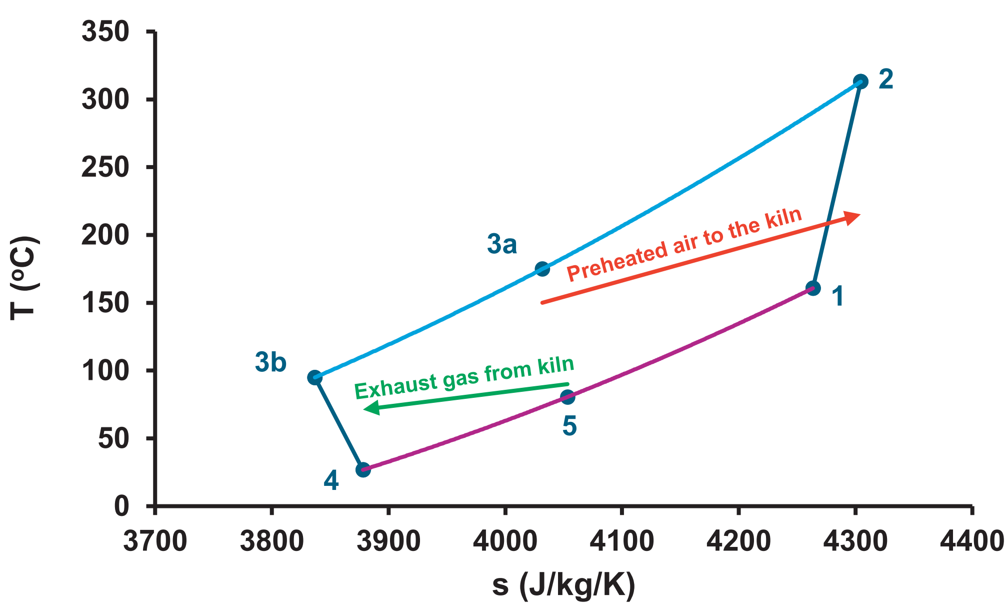

(b)

Fig. 3. (a) Thermodynamic cycle of the examined Reverse Brayton HTHP, (b) T-S diagram of the cycle.

Methodology and implementation

Parametric optimization and dynamic analysis

In this section, the main steps followed regarding parametric optimization and the dynamic analysis are presented in detail. The operating conditions and the main assumptions for each analysis are also given.

Regarding the parametric optimization analysis, the main objective was to maximize the HTHP's performance (COP) by adjusting the mass flow rate of the air in the closed circuit. Specifically, the optimization was conducted for eleven different inlet temperatures of preheated air supplied to the HTHE, ranging from 100 °C to 200 °C in 10 °C increments. For each of these inlet temperature values, multiple working medium mass flow rates were tested within the range of 3.0 kg/s to 10.0 kg/s. This process facilitated the calculation of the optimum working fluid mass flow rate for each inlet temperature, using the maximization of both the COP and exergy efficiency as the primary criteria. Consequently, from this analysis, it was feasible to develop a mathematical expression that provides the optimum working medium mass flow rate as a function of the preheated air inlet temperature. This mathematical expression was subsequently integrated into the dynamic analysis model to determine optimal operation.

As far as the dynamic analysis is concerned, the HTHP was assumed to operate in real operating conditions according to representative measured data taken directly from the KEBE industry. This data includes the temperature of the inlet preheated air (exiting the cooling zone and entering the HTHE) and the inlet exhaust gases (exiting the preheating zone and entering the LTHE). The measured data covered a continuous operating period of 168 consecutive hours (one week) from May 18th to 24th. This period was selected as representative among several time series of yearly operation for the specific industrial site, considering that no significant fluctuations appeared during the examined year. It is important to mention that the inlet preheated air temperature ranges from 106.8 °C to 179 °C, corresponding to a typical week fluctuation (see Fig. 9c in section 3.2), while the inlet exhaust gases temperature appears to have negligible fluctuations during the examined period, according to the available data taken from the industry, with a representative mean value of 90 °C. This occurs because the kiln combustion system is regulated to adjust natural gas consumption according to the production load and the temperature of the preheated combustion air through a centralized automatic control system. In this way, significant energy waste is avoided while maintaining an almost constant flue gas temperature [30]. Hence, by implementing the working medium mass flow rate mathematical expression developed through the optimization procedure, it was possible to study the dynamic operation of the HTHP for real operating data of the industry, considering the optimum working medium mass flow rate values for each operating hour according to the fluctuation of the inlet preheated air temperature during the examined time period.

It should be mentioned that the mass flow rate of the preheated air (HTHE secondary circuit) and the exhaust gases (LTHE primary circuit) were considered to be $\dot{\mathbf{m}}_{\mathbf{PA,in}} = 15\,\mathbf{kg/s}$ and $\dot{\mathbf{m}}_{\mathbf{EG,in}} = 20\,\mathbf{kg/s}$ respectively, while the exhaust gas inlet temperature took the value of 90 °C in both parametric optimization and dynamic analysis. The useful thermal power output ($\dot{\mathbf{Q}}_{\mathbf{out}}$) was also considered to be steady and equal to 1,000 kW_{th} in all analyses. All the prementioned parameters remained constant for the whole examined period.

The main assumptions of the study regard the effectiveness of the examined heat exchangers, the isentropic efficiency of the compressor and the turbine, as well as the low pressure of the cycle. More specifically, the effectiveness of all the HTHP heat exchangers (HTHE, REC and LTHE) as well as the isentropic efficiency of both the turbine and the compressor were considered to be equal with 85%, which is a reasonable value according to the ranges studied in Ref. [22]. It is remarkable to mention that the compressor's isentropic efficiency was selected to be the same as the turbine's isentropic efficiency, despite the fact that usually during actual operation of Brayton power cycles the turbine is more efficient. However, in the Reverse Brayton cycle, the compressor is a more important component because it treats higher amounts of power, thus the isentropic efficiencies were selected to be identical in the reference case presented, complemented by a parametric study on variable isentropic efficiencies for the compressor and the turbine as this is presented later in the manuscript (section 3.1). Moreover, selecting equal isentropic efficiencies simplifies the thermodynamic formulation and reduces the number of independent parameters in the model. This allows the analysis to focus on the cycle-level behaviour (e.g., pressure ratio, heat input, mass flow rate, and temperature levels) rather than on the performance differences between individual turbomachinery components. The electromechanical conversion efficiency of the compressor's motor was taken equal to 98%, including the mechanical losses for driving the compressor-turbine shaft [24].

Mathematical formulation

The main equations that were utilized for the present analysis are provided in this paragraph. These equations mainly regard the thermal and thermodynamic equilibria of the working mediums in the three heat exchangers of the examined HTHP, as well as the effectiveness and efficiency characteristics of all the components involved. All the equations given here constitute the core of the model described in paragraph 2.2.3.

To begin with, for the needs of the present analysis, it was necessary to define the effectiveness of HTHE, LTHE and REC devices. The respective definitions were put forward considering the NTU method with regard to the heat transfer. Equation (1) presents the effectiveness of the HTHE device.

$$\mathbf{eff}_{\mathbf{HTHE}} = \frac{\dot{\mathbf{Q}}_{\mathbf{HTHE}}}{\dot{\mathbf{Q}}_{\mathbf{max,HTHE}}} \tag{1}$$

Parameter ($\dot{\mathbf{Q}}_{\mathbf{HTHE}}$) which is provided through Eq. (2) expresses the thermal power that is conveyed from the HTHP air working medium to the preheated air.

$$\begin{aligned}\dot{\mathbf{Q}}_{\mathbf{HTHE}} &= \dot{\mathbf{Q}}_{\mathbf{out}} = \dot{\mathbf{m}}_{\mathbf{PA}}\cdot\left(\mathbf{h}_{\mathbf{PA,out}} - \mathbf{h}_{\mathbf{PA,in}}\right) = \dot{\mathbf{m}}_{\mathbf{PA}}\cdot\mathbf{Cp}_{\mathbf{PA}}\cdot\left(\mathbf{T}_{\mathbf{PA,out}} - \mathbf{T}_{\mathbf{PA,in}}\right)\\ &= \dot{\mathbf{m}}_{\mathbf{R}}\cdot\left(\mathbf{h}_2 - \mathbf{h}_{3a}\right)\end{aligned} \tag{2}$$

The ($\dot{\mathbf{Q}}_{\mathbf{max,HTHE}}$) parameter represents the maximum possible thermal power which could ideally be transferred to the preheated air, considering the minimum heat capacity rate of the two streams of the HTHE as Eq. (3) recommends.

$$\dot{\mathbf{Q}}_{\mathbf{max,HTHE}} = \mathbf{C}_{\mathbf{min,HTHE}}\cdot\left(\mathbf{T}_2 - \mathbf{T}_{\mathbf{PA,in}}\right) \tag{3}$$

where:

$$\mathbf{C}_{\mathbf{min,HTHE}} = \mathbf{min}\left(\mathbf{C}_{\mathbf{PA}}, \mathbf{C}_{\mathbf{R,HTHE}}\right) \tag{4}$$

$$\mathbf{C}_{\mathbf{R,HTHE}} = \dot{\mathbf{m}}_{\mathbf{R}}\cdot\mathbf{Cp}_{\mathbf{R,HTHE}} \tag{5}$$

$$\mathbf{C}_{\mathbf{PA}} = \dot{\mathrm{m}}_{\mathbf{PA}}\cdot\mathbf{Cp}_{\mathbf{PA}} \tag{6}$$

Eq. (7) presents the effectiveness of the LTHE device:

$$\mathbf{eff}_{\mathbf{LTHE}} = \frac{\dot{\mathbf{Q}}_{\mathbf{LTHE}}}{\dot{\mathbf{Q}}_{\mathbf{max,LTHE}}} \tag{7}$$

Parameter $\dot{\mathbf{Q}}_{\mathbf{LTHE}}$ corresponds to the thermal power that is conveyed from the exhaust gases to the HTHP working medium exchanged and it is given by Eq. (8).

$$\begin{aligned}\dot{\mathbf{Q}}_{\mathbf{in}} &= \dot{\mathbf{Q}}_{\mathbf{LTHE}} = \dot{\mathbf{m}}_{\mathbf{EG}}\cdot\left(\mathbf{h}_{\mathbf{EG,in}} - \mathbf{h}_{\mathbf{EG,out}}\right) = \dot{\mathbf{m}}_{\mathbf{EG}}\cdot\mathbf{Cp}_{\mathbf{EG}}\cdot\left(\mathbf{T}_{\mathbf{EG,in}} - \mathbf{T}_{\mathbf{EG,out}}\right)\\ &= \dot{\mathbf{m}}_{\mathbf{R}}\cdot\left(\mathbf{h}_5 - \mathbf{h}_4\right)\end{aligned} \tag{8}$$

The parameter of $\dot{\mathbf{Q}}_{\mathbf{max,LTHE}}$ refers to the maximum possible thermal power which could be transferred ideally to the air working medium of the HTHP, considering the minimum heat capacity rate of the two streams in the heat exchanger, as it is presented in Eq. (9).

$$\dot{Q}_{max,LTHE} = C_{min,LTHE} \cdot (T_{EG,in} - T_4) \quad (9)$$

where:

$$C_{min,LTHE} = \min(C_{EG}, C_{R,LTHE}) \quad (10)$$

$$C_{R,LTHE} = \dot{m}_R \cdot Cp_{R,LTHE} \quad (11)$$

$$C_{EG} = \dot{m}_{EG} \cdot Cp_{EG} \quad (12)$$

The same rationale was followed for recuperator effectiveness, which is defined according to Eq. (13):

$$eff_{REC} = \frac{\dot{Q}_{REC}}{\dot{Q}_{max,REC}} \quad (13)$$

Parameter $\dot{Q}_{REC}$ represents the thermal power that is exchanged between the low-pressure and the high-pressure stream in the REC device and it is calculated as described in Eq. (14):

$$\dot{Q}_{REC} = \dot{m}_R \cdot (h_{3a} - h_{3b}) = \dot{m}_R \cdot Cp_{R,REC,low} \cdot (T_1 - T_5) = \dot{m}_R \cdot (h_5 - h_1) \quad (14)$$

The $\dot{Q}_{max,REC}$ parameter corresponds to the maximum thermal power which could be transferred ideally to the low-pressure stream, considering the minimum heat capacity rate of the two streams, as Eq. (15) suggests.

$$\dot{Q}_{max,REC} = C_{min,REC} \cdot (T_{3a} - T_5) \quad (15)$$

where:

$$C_{min,REC} = \min(C_{R,REC,low}, C_{R,REC,high}) \quad (16)$$

$$C_{R,REC,low} = \dot{m}_R \cdot Cp_{R,REC,low} \quad (17)$$

$$C_{R,REC,high} = \dot{m}_R \cdot Cp_{R,REC,high} \quad (18)$$

The combination of Eqs. (1)–(3), Eqs. (7)–(9) and Eqs. (13)–(15) provide Eqs. (19)–(21), which will be utilized properly in the developed model.

$$T_2 = T_{PA,in} + \frac{\dot{m}_{PA} \cdot (h_{PA,out} - h_{PA,in})}{C_{min,HTHE} \cdot eff_{HTHE}} \quad (19)$$

$$h_5 = h_4 + eff_{LTHE} \cdot C_{min,LTHE} \cdot (T_{EG,in} - T_4) \quad (20)$$

$$h_1 = h_5 + eff_{REC} \cdot C_{min,REC} \cdot (T_{3a} - T_5) \quad (21)$$

Another useful calculation is given in Eq. (22) as regards the calculation of the outlet temperature of the preheated air from the HTHE:

$$T_{PA,out} = T_{PA,in} + \frac{\dot{Q}_{HTHE}}{Cp_{PA,HTHE} \cdot \dot{m}_{PA}} \quad (22)$$

The isentropic efficiency expressions for the compressor and the turbine components of the HTHP are given in Eq. (23) and (24), respectively:

$$\eta_{is,C} = \frac{h_{2,is} - h_1}{h_2 - h_1} \quad (23)$$

$$\eta_{is,T} = \frac{h_{3b} - h_4}{h_{3b} - h_{4,is}} \quad (24)$$

Eqs. (25) and (26) calculate the work of the compressor and the turbine, while Eq. (27) provides the mechanical work needed to be added by the compressor's motor. Equation (28) calculates the electrical power needed for the compressor's operation.

$$\dot{W}_C = \dot{m}_R \cdot (h_2 - h_1) \quad (25)$$

$$\dot{W}_T = \dot{m}_R \cdot (h_{3b} - h_4) \quad (26)$$

$$\dot{W}_{C,motor} = \dot{W}_C - \dot{W}_T \quad (27)$$

$$P_{el} = \frac{\dot{W}_{C,motor}}{\eta_{elm}} \quad (28)$$

As was mentioned in section 2.3.1, the electromechanical conversion efficiency in Eq. (28) considers the global mechanical losses of the compressor and the turbine. The coefficient of performance of the HTHP (COP) is available in Eq. (29).

$$COP = \frac{\dot{Q}_{HTHE}}{\dot{W}_{C,motor}} \quad (29)$$

The pressure ratio of the compressor and the turbine was also considered in the framework of the specific study. Their expressions are available in Eqs. (30) and (31) respectively.

$$PR_C = \frac{p_2}{p_1} \quad (30)$$

$$PR_T = \frac{p_{3b}}{p_4} \quad (31)$$

Exergy efficiency is within the scope of the present analysis and thus, all the necessary parameters regarding its calculation are presented here. Exergy efficiency is defined as the ratio of the maximum useful power that could be produced ideally (Ex_{out}) to the exergy input in the system ($Ex_{in} + Ex_{el,motor}$). The parameter (Ex_{out}) expresses the useful power output that could be obtained by a Carnot power engine if the useful power produced by the HTHP ($\dot{Q}_{out}$) were considered as an input to the engine. The sum of (Ex_{in}) and ($Ex_{el,motor}$) constitutes the power output of a Carnot engine if the inlet thermal power from the exhaust gases and the input power from the compressor's motor are assumed as inputs to the engine. Eqs. (36)–(39) provide the expressions of all the prementioned parameters [24,31].

$$\eta_{ex} = \frac{Ex_{out}}{Ex_{in} + Ex_{el}} \quad (32)$$

$$Ex_{out} = \dot{m}_{PA} \cdot Cp_{PA} \cdot (T_{PA,out} - T_{PA,in}) - \dot{m}_{PA} \cdot Cp_{PA} \cdot T_{ref} \cdot \ln\left(\frac{T_{PA,out}}{T_{PA,in}}\right) \quad (33)$$

$$Ex_{in} = \dot{m}_{EG} \cdot Cp_{EG} \cdot (T_{EG,in} - T_{EG,out}) - \dot{m}_{EG} \cdot Cp_{EG} \cdot T_{ref} \cdot \ln\left(\frac{T_{EG,in}}{T_{EG,out}}\right) \quad (34)$$

$$Ex_{el} = P_{el} \quad (35)$$

The reference temperature in the particular study is selected to take the value of 298.15 K [31], while all the temperatures in Eqs. (36)-(39) must be set in Kelvin (K).

Developed model

In this study, the optimization and dynamic calculations were performed using a detailed analytical model developed in MATLAB [32]. The model was designed to incorporate all necessary thermodynamic parameters and operating conditions of the examined closed-loop Reverse Brayton HTHP cycle.

Importantly, the model was structured to perform detailed thermodynamic calculations while dynamically accounting for the pressure-drop effects introduced by the heat exchangers, which depend directly on the working-medium mass flow rate. The pressure-drop correlations, as presented in Eqs. (36)-(39) were derived from a comprehensive parametric analysis performed using the commercial CFD software UNILAB [33].

$$\mathbf{Dp_{HTHE}} = \left(0.06452\cdot\dot{\mathbf{m}}_{\mathbf{R}}^{\ 2} + 0.21452\cdot\dot{\mathbf{m}}_{\mathbf{R}} - 0.22679\right)\bullet 10^3 \tag{36}$$

$$\mathbf{Dp_{REC,high}} = \left(0.06054\cdot\dot{\mathbf{m}}_{\mathbf{R}}^{\ 2} + 0.21625\cdot\dot{\mathbf{m}}_{\mathbf{R}} - 0.24732\right)\bullet 10^3 \tag{37}$$

$$\mathbf{Dp_{REC,\ low}} = \left(0.01379\cdot\dot{\mathbf{m}}_{\mathbf{R}}^{\ 2} + 0.07615\cdot\dot{\mathbf{m}}_{\mathbf{R}} - 0.0872\right)\bullet 10^3 \tag{38}$$

$$\mathbf{Dp_{LTHE}} = \left(-0.00295\cdot\dot{\mathbf{m}}_{\mathbf{R}}^{\ 3} + 0.1072\cdot\dot{\mathbf{m}}_{\mathbf{R}}^{\ 2} - 0.24519\cdot\dot{\mathbf{m}}_{\mathbf{R}} + 0.67952\right)\bullet 10^3 \tag{39}$$

UNILAB is a commercially available and widely used simulation tool that has been extensively validated for real-world engineering applications, including turbulent internal flow and heat transfer problems. It is commonly employed in the design and performance analysis of fin-and-tube heat exchangers for industrial applications. Therefore, the correlations derived from this software are considered reliable within the defined geometric configurations and the Reynolds number ranges examined in this work.

For the purposes of the present analysis, a fin-and-tube heat exchanger configuration was adopted. Table 2 summarizes the main geometrical characteristics that vary among the examined cases, along with the corresponding Reynolds number ranges obtained from the UNILAB calculations for each geometry. It should be noted that the inner and outer diameters of the coil tubing were fixed at 36.7 mm and 42.2 mm, respectively, while the fin length and fin pitch were set to 3000 mm and 6 mm. These parameters were kept constant across all the heat exchangers considered in the analysis.

As far as the developed code is concerned, it is mainly based on solving a complex system of equations via iterations. All the thermodynamic properties are calculated using CoolProp libraries by using specific functions in the MATLAB environment [34]. It has to be mentioned that the exhaust gases were considered as air as far as the thermodynamic analysis is concerned. This is a reasonable assumption since the specific heat capacity of the flue gases is near that of air. Further information and justification regarding this assumption is available in Appendix A.

According to the adopted methodological approach, several parameters should be defined before iteratively solving the set of equations. Specifically, Eq. (22) is utilized to calculate the outlet temperature of the preheated air stream in the HTHE ($\mathbf{T_{PA,out}}$). In addition, the temperature immediately after the compressor at point 2 of the cycle ($\mathbf{h_2}$), as illustrated in Fig. 3, is calculated using Eq. (19), while Eq. (2) is applied to calculate the enthalpy at point 3a ($\mathbf{h_{3a}}$). More specifically, an initial value for the turbine exit temperature ($\mathbf{T_4}$) is first assumed. Next, the enthalpy of the air working medium after the LTHE ($\mathbf{h_5}$) is calculated using Eq. (20), and the enthalpy before the compressor ($\mathbf{h_1}$) is calculated through Eq. (21). The calculation of ($\mathbf{h_1}$) enables the determination of entropy at the same point (s_1), since the pressure there ($\mathbf{p_1}$) is supposed to be fixed at 1 bar. As a next step, the expression of the compressor's isentropic efficiency, given in Eq. (23), is utilized to calculate the isentropic enthalpy at point 2 ($\mathbf{h_{2,is}}$). This enables the determination of the total pressure at point 2 ($\mathbf{p_2}$) using the CoolProp libraries, with $\mathbf{h_{2,is}}$ and $\mathbf{s_1}$ as inputs. The enthalpy at point 3b ($\mathbf{h_{3b}}$) is defined using the last two parts of Eq. (14). The analysis then proceeds with the calculation of the total pressure at points 3α, 3b, 4 and 5 (see Fig. 3) in [Pa], by using the parametric mathematical expressions for the pressure drop as a function of the air working medium mass flow rate in the three heat exchangers of the HTHP, as described in Eqs. (36)-(39).

It is significant to note here that for the REC device, it was necessary to define separate pressure drop functions for the high-pressure and low-pressure stages, since the enclosed air passes through both REC circuits. Additionally, the HTHP air working medium is assumed to flow in the tube side of both the HTHE and the LTHE, while in the case of the REC heat exchanger, the tube side corresponds to the low-pressure circuit and the fin side to the high-pressure circuit. After accounting for the pressure drops and calculating the total pressure at each point, the entropy at point 3b ($\mathbf{s_{3b}}$) is determined using the CoolProp libraries with $\mathbf{p_{3b}}$ and $\mathbf{h_{3b}}$ as inputs. Once the entropy at point 3b and the pressure at point 4 are known, the isentropic enthalpy $\mathbf{h_{4,is}}$ can be calculated using CoolProp libraries. Finally, Eq. (24) is solved for the actual enthalpy $\mathbf{h_4}$, and the updated temperature at point 4 ($\mathbf{T_{4,new}}$) is obtained via CoolProp. This new temperature is then used as an input in Eq. (20), and the iterations are repeated until convergence is achieved. It should be noted that this iterative procedure is applied both in the parametric optimization and in the dynamic analysis. The developed model exhibits a mean real-time calculation of 305.81 s (5.1 min) for the optimization analysis and 130.11 s (2.17 min) for the dynamic analysis, with a total of 781 and 336 iterations, respectively.

Table 2
Geometrical characteristics and Reynolds number ranges of the adopted heat exchangers.

Heat exchanger	HTHE	LTHE	REC (high pressure)	REC (low pressure)
Tubes per row	40	40	20	
Number of rows	8	10	40	
Number of circuits	160	200	200	
HTHP circuit side	Coil side	Coil side	Coil side	Fins side
Reynolds number range (x10^4)	1.9 –6.2	2.7 –9.0	1.4 –4.7	1.2

Verification

Given that experimental data of the HTHP are not yet available and since the current study focuses on the design and dimensioning of the proposed electrified system to substitute the currently used NG system, a secondary model developed in the software EBSILON® Professional was utilized to verify the accuracy and the validity of the present MATLAB model. EBSILON® Professional [35] is a commercial software, which can be used for planning, monitoring and optimization of power plants and other thermodynamic processes. The equations and physics used for the calculation of each component have been documented. This software has been validated through experimental results in various studies, as in study [36], considering HTHP systems and thus it constitutes a reliable tool for the present analysis.

The operating data that were utilized for the verification procedure were considered according to an initial dimensioning scenario, which was developed in the framework of the EEETHOS project. Specifically, the inlet exhaust gas temperature and the respective preheated air temperature were assumed to be 85 °C and 230 °C respectively, with the useful output to take the value of 1090 kW_{th}. The mass flow rate of the exhaust gases and the preheated air stream were considered as inputs, set equal to 21.83 kg/s and 15 kg/s, with both the effectiveness of each heat exchanger and the isentropic efficiency of the compressor and the turbine to be considered equal to 85%. The comparison of the two models was conducted for eight different mass flow rate values of the enclosed to the cycle air (3–10 kg/s with 1 kg/s step) under steady state conditions. The results of the present verification are presented in detail in Fig. 4 for all the examined cases.

As observed in Fig. 4, the results from the MATLAB model demonstrate sufficient agreement with the reference data, with a mean deviation below 0.4% in all cases and a maximum deviation of 0.60% observed for the turbine work ($\dot{\mathbf{W}}_{\mathbf{T}}$) comparison. Particularly, a perfect match occurs between the two models for the COP (deviation $\leq$ 0.38%), the electrical power consumption (deviation $\leq$ 0.43%), the inlet thermal power (deviation $\leq$ 0.25%), the turbine work (deviation $\leq$ 0.60%), and

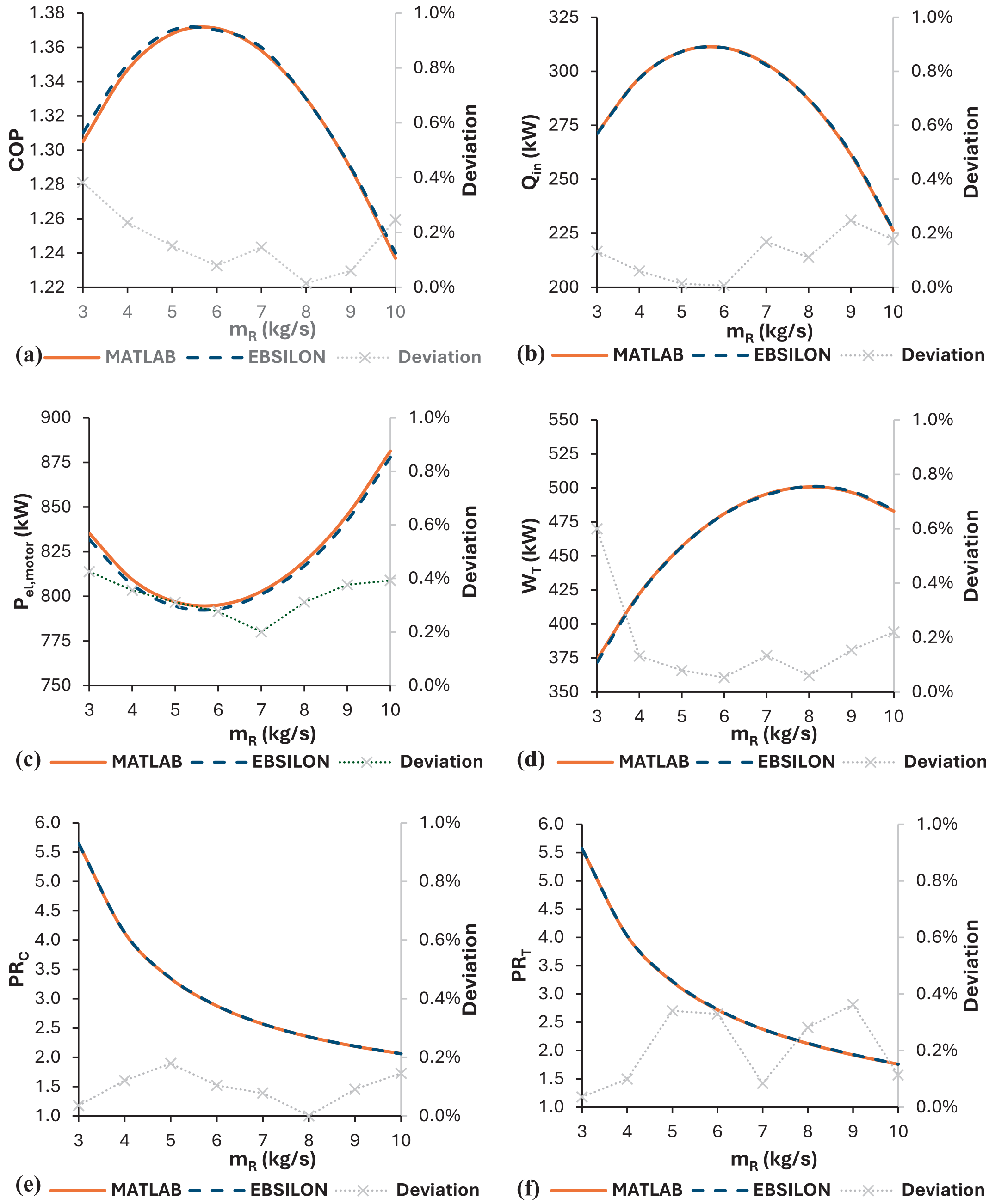

Fig. 4. Verification of the developed model: (a) Coefficient of Performance (COP), (b) Inlet thermal power (Q_{in}), (c) Compressor's motor electrical power ($P_{el,motor}$), (d) Mechanical work from turbine (W_T), (e) Pressure Ratio of the compressor (PR_C) and (f) Pressure Ratio of the turbine (PR_T) as a function of the working medium mass flow rate.

the pressure ratios of the compressor and the turbine (deviation $\leq$ 0.18% and 0.36%, respectively). Hence, the developed model accurately captures all the thermodynamic phenomena that take place in the examined HTHP and provides reliable results. It should be mentioned that the validated model was employed for both the optimization and dynamic analyses.

Results and Discussion

The main results of the present analysis are presented in a dedicated section. Emphasis is placed on the parametric optimization of the HTHP's air working-medium mass flow rate in terms of performance (COP maximization), with a focus on maximizing the system's performance. The dynamic analysis results are also included in this section.

Preliminary sensitivity analysis

In this section, a preliminary analysis is conducted in order to investigate the effect of the important design parameters' variation. Thus, the isentropic efficiency of the compressor and the turbine, as well as the effectiveness of the heat exchangers, were taken at several values (0.70 to 0.90 with a step of 0.05) in order to evaluate how the COP is affected. Fig. 5 illustrates the variation of the COP as a function of the mass flow rate for several different values of the heat exchangers' effectiveness and the two isentropic efficiencies of the compressor and the turbine. The analysis was conducted for the inlet preheated air temperature of 150 °C.

As is observed from Fig. 5, the COP is enhanced with the increment of the isentropic efficiencies of the compressor and the turbine, as well as of

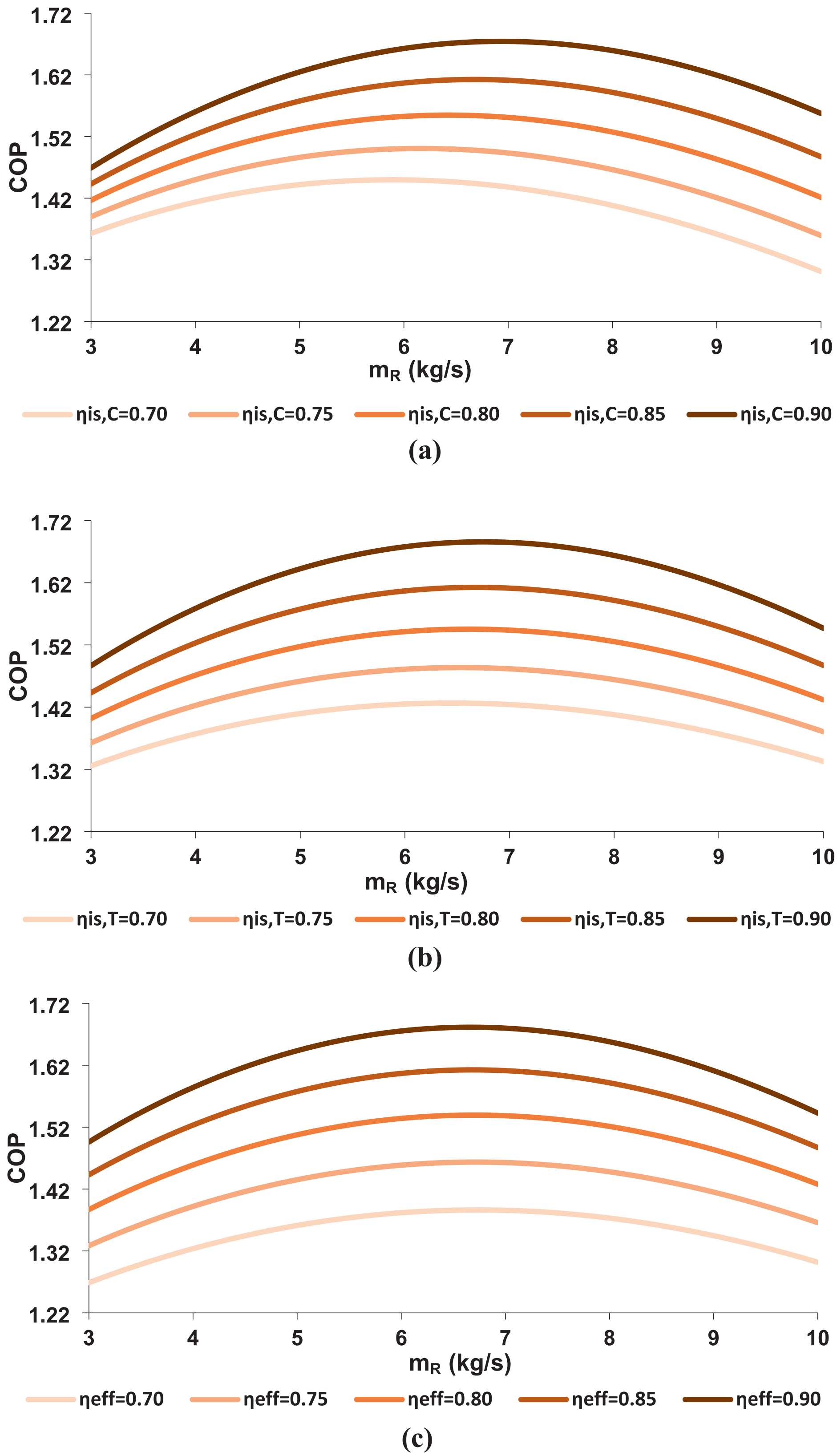

Fig. 5. Sensitivity analysis for $T_{PA,in}$ = 150 °C: COP variation as a function of (a) $\eta_{is,C}$, (b) $\eta_{is,T}$ and (c) η_{eff}.

the heat exchangers' effectiveness. Generally, COP takes reasonably higher values when each one of the examined design parameters ($\eta_{is,C}$, $\eta_{is,T}$ and η_{eff}) increases. It is worth noticing that the COP maximum increases with the increment of the compressor's isentropic efficiency, while this seems to be more intense than in the turbine isentropic efficiency case, in which the respective rise appears to be smoother.

Parametric optimization

Parametric optimization focuses on the detailed examination of the HTHP operation, considering several different operating preheated air temperature inlet levels between 100 °C and 200 °C and variation of the working medium mass flow rate in the range of 3–10 kg/s in each of the examined temperatures. Fig. 6 provided the coefficient of performance and the exergy efficiency (Fig. 6a), the work of the turbine and the remaining work needed for the compressor (Fig. 6b), as well as the inlet thermal power and the outlet temperature of the exhaust gases (Fig. 6c) as a function of the air working medium mass flow rate for each one of the examined inlet preheated air temperatures.

As depicted in Fig. 6a, the COP decreases as the inlet temperature of the preheated air increases. This trend is expected, as higher inlet temperatures require greater compressor work to deliver the same thermal power output in the HTHE. Conversely, the exergy efficiency increases with higher preheated-air inlet temperatures, which is reasonable given that the thermal quality of the heat supplied to the cycle improves.

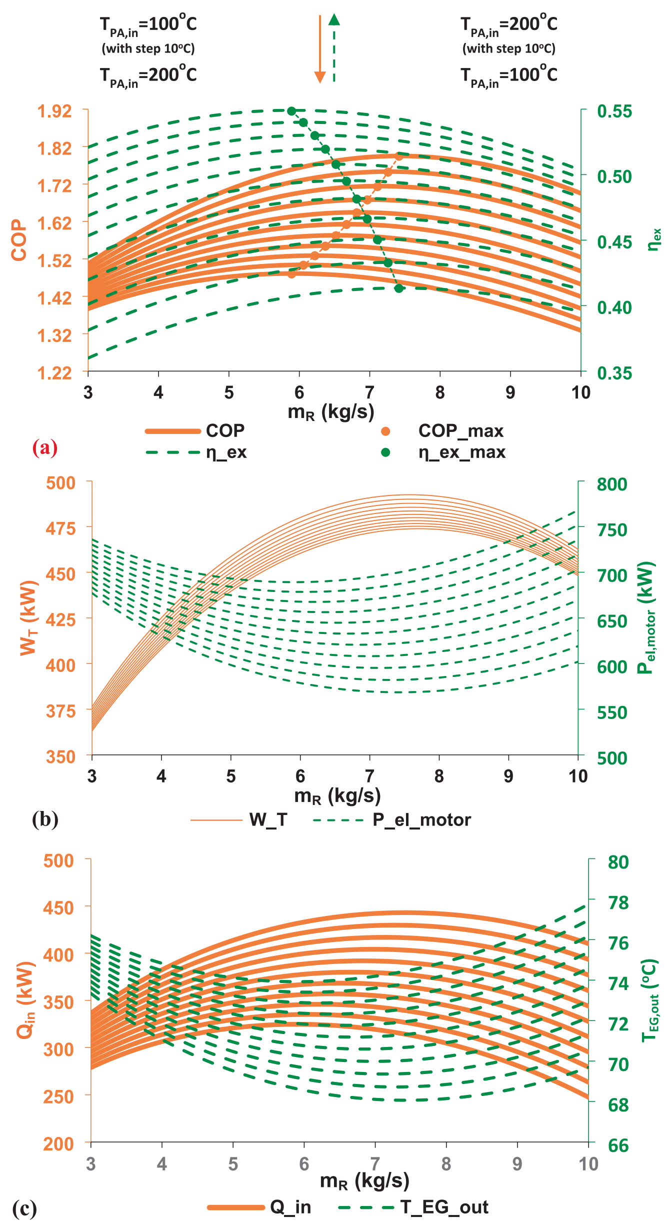

Fig. 6. Parametrical optimization results: (a) COP and η_{ex}, (b) W_T and $W_{C,motor}$ and (c) Q_{in} and $T_{EG,out}$.

An additional noteworthy observation is that the optimal mass flow rate decreases as the preheated-air temperature rises. This occurs because the temperature difference between the inlet and outlet of the HTHE on the closed-circuit side increases with higher inlet temperatures. Finally, it is important to highlight that, for each preheated-air temperature considered, the maximum COP and maximum exergy efficiency are achieved at the same mass flow rate.

Fig. 6b illustrates the influence of the working-medium mass flow rate and the inlet temperature of the preheated air on the turbine work output and the compressor-motor electrical power demand. Notably, the turbine work reaches its maximum at a mass flow rate of approximately 7.6 kg/s, regardless of the preheated-air inlet temperature, with values ranging between roughly 350 and 500 kW_{th}. The effect of the inlet temperature is comparatively small, as the variation in turbine work near the optimal operating region is limited to about 25 kW. This observation confirms the strong dependence of turbine work on the mass flow rate.

In contrast, the compressor-motor electrical power ($\mathbf{P_{el,motor}}$) reaches a minimum at the same mass flow rate that maximizes the COP, which is consistent with the fact that the electrical power consumption is inversely related to the COP.

From Fig. 6c, it is evident that the inlet thermal power from the LTHE to the cycle ($\dot{\mathbf{Q}}_{\mathbf{in}}$) reaches its maximum values at the same mass flow rates where the COP is also maximized. An increase in the preheated air inlet temperature has a remarkable impact on $\dot{\mathbf{Q}}_{\mathbf{in}}$, causing it to decrease. This is expected, since higher preheated air inlet temperature leads to higher turbine outlet temperatures, which in turn reduce the effective heat capacity of the LTHE, given that the exhaust gases inlet temperature is assumed to be constant. As far as the outlet exhaust gases temperature, it exhibits a reverse behavior compared to $\dot{\mathbf{Q}}_{\mathbf{in}}$, which aligns with the predictions of Eq. (8).

Fig. 7 presents the main output of the optimization procedure, which is not other than the optimum values of the closed-circuit air mass flow rate for each one of the examined inlet temperatures of the preheated air. As observed, the optimum mass flow rate decreases approximately linearly as the inlet preheated air temperature increases. This diagram enabled the derivation of an important empirical correlation describing this relationship. This mathematical expression is available in Eq. (40) and will be utilized for the dynamic analysis that follows.

$$\dot{m}_{R,opt} = -0.015 \cdot T_{PA,in} + 8.923\,, \quad R^2 = 0.99725 \tag{40}$$

Effect of the useful thermal output

In this section, a parametric investigation is conducted to examine the effect of the useful thermal output on the performance of the

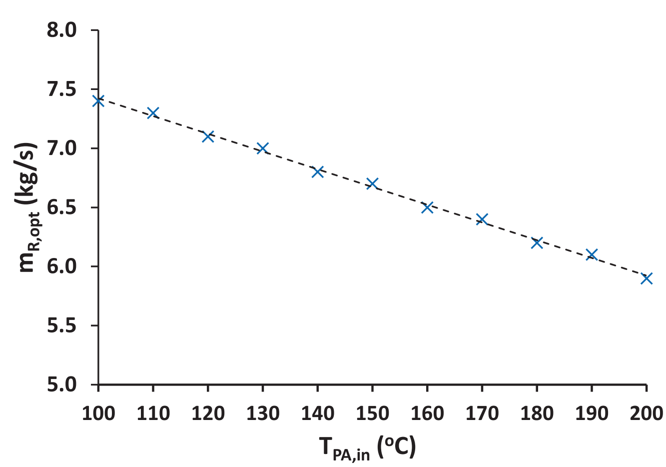

Fig. 7. Optimum working medium mass flow rate for each preheated air inlet temperature.

proposed HTHP, as well as on the optimal mass flow rate determined through the optimization process. To this end, five different useful thermal output levels were considered, ranging from 500 to 1500 kW_{th} with a step of 250 kW_{th}, and the corresponding optimal mass flow rate was determined for each case. The analysis was carried out considering steady state conditions and a preheated air inlet temperature of 150 °C. Fig. 8 presents the results of this parametric analysis, illustrating the COP curves along with the variation of the optimal mass flow rate as a function of the useful thermal output.

As illustrated in Fig. 8a, the optimal mass flow rate increases with increasing useful heat output. This behaviour can be explained by the fact that, as the heat demand rises, a higher mass flow rate is required to supply the additional thermal energy while maintaining lower specific mechanical work requirements for the compressor. It is also noteworthy that the COP reaches higher maximum values at lower heat demand levels. This occurs because the pressure ratio tends to decrease when the required high-temperature heat output is lower, resulting in reduced mechanical work consumption by the compressor, as also indicated in Fig. 8b.

Dynamic investigation

In this section, the dynamic analysis results are presented. The operation of the examined HTHP system was evaluated under dynamic, real-life operating conditions based on data provided by the KEBE industry for a continuous operating period of 168 h, with measurements recorded every 10 min. The preheated air inlet temperature fluctuated between 105 °C and 180 °C, while the exhaust gases inlet temperature was assumed to be constant at 90 °C, as only minor variations were observed during the examined period within the range of 85–95 °C. The mass flow rate of the air working medium within the cycle was set to its optimal values, determined from the timeseries of the inlet preheated air temperature using Eq. (40). More specifically, real-time adjustment of the air working medium mass flow rate was considered for the maximization of the COP. This control strategy is reasonable and engineeringly feasible considering the utilization of Variable Speed Drive (VSD) technology for the compressor's motor, which typically provides response times on the order of seconds and flow control accuracy within ± 1–3%, which is sufficient within the requirements for COP optimization in the present case, given the relatively large thermal inertia of

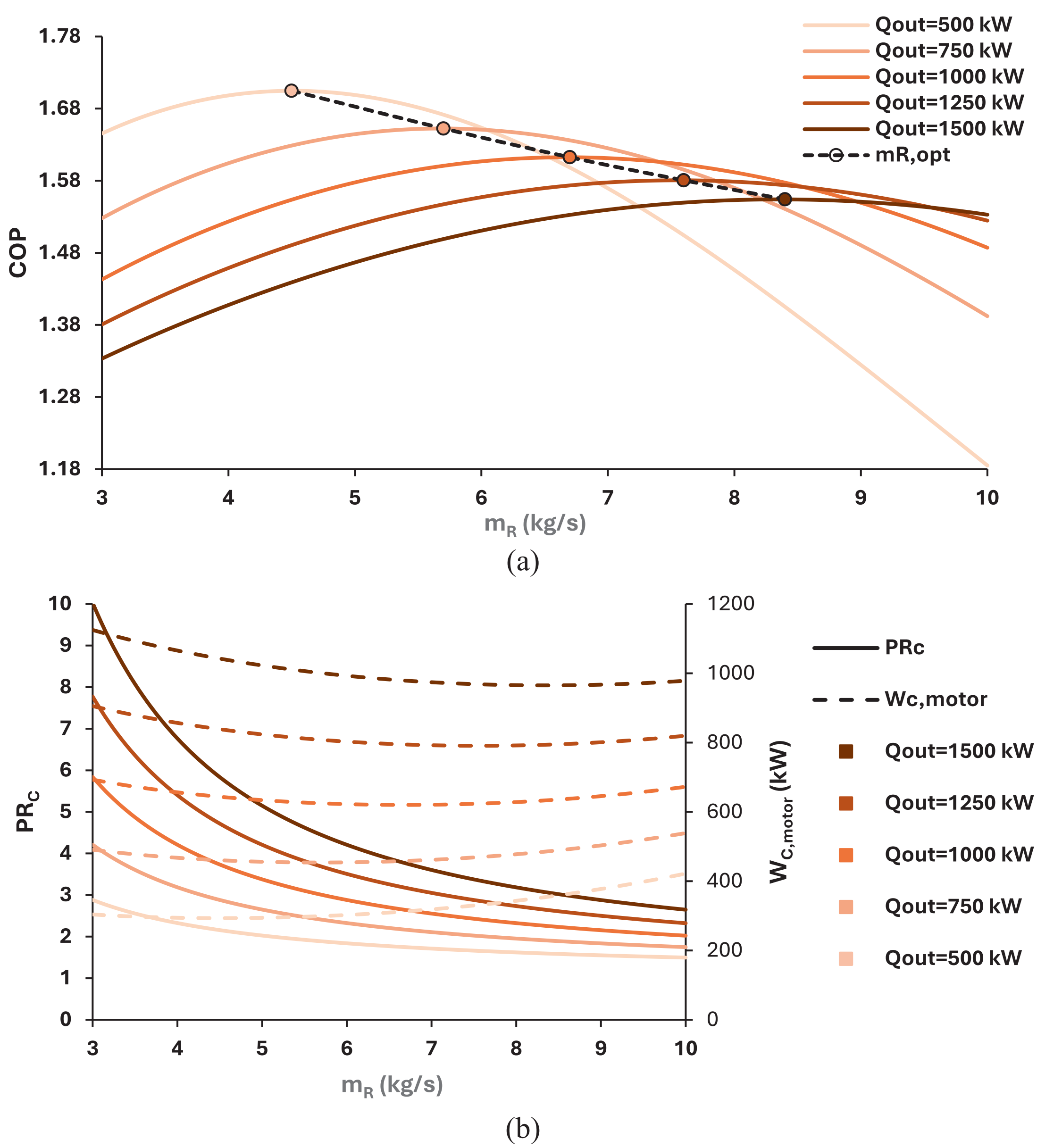

Fig. 8. Parametric optimization for five different Q_{out} values and $T_{PA,in}$ = 150 °C: (a) COP and (b) PR_C and $W_{C,motor}$.

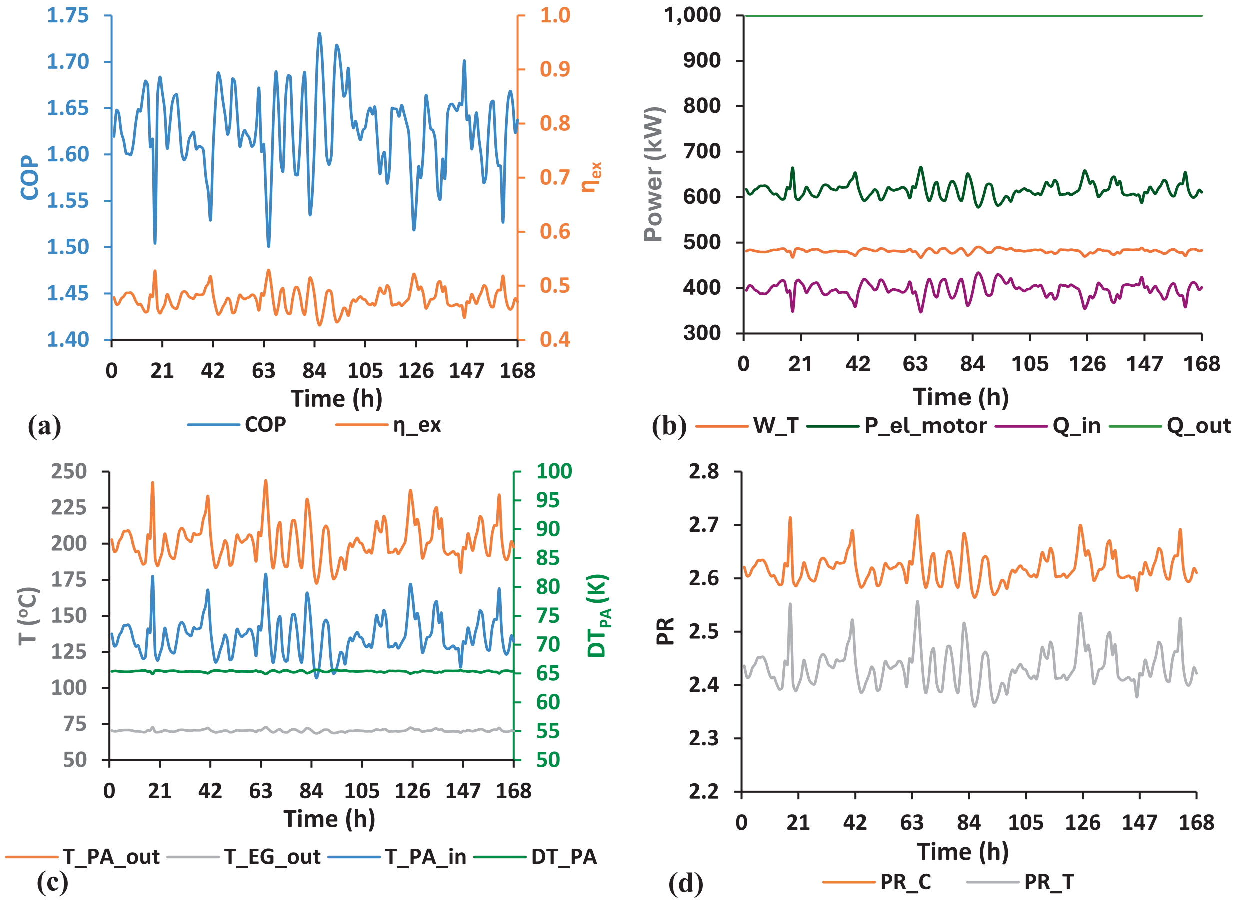

Fig. 9. Dynamic analysis results: a) COP and Exergy efficiency, b) W_T, $P_{el,motor}$, Q_{in}, Q_{out}, c) $T_{PA,in}$, $T_{PA,out}$, $T_{EG,out}$, DT_{PA} and d) PR_C, PR_T as a function of time for 168 h of operation.

kiln-integrated systems. Such control approaches are already widely applied in industrial HVAC and waste heat recovery systems, accompanied by technical feasibility and cost-effectiveness due to the maturity and moderate cost of VSD technology [37,38].

Fig. 9 provides the main results of the dynamic analysis, highlighting all power equilibria, the compressor and turbine pressure ratios, the COP and the exergy efficiency, as well as the outlet temperatures of both the preheated air and the exhaust gases.

As shown in Fig. 9, the mean operation of the HTHP remains nearly steady during the examined period, with fluctuations driven primarily by variations in the preheated air inlet temperature. According to Fig. 9a, the COP ranges from approximately 1.50 to 1.75, while the exergy efficiency is between 0.43 and 0.53. It is also evident that the exergy efficiency reaches its maximum when the COP attains its lower values, a trend also observed in the optimization analysis (see Fig. 6a). In Fig. 9b, the inlet thermal power supplied to the cycle through the LTHE seems to show a relatively smooth variation, further confirming its independence from the preheated air inlet temperature, as previously observed in the optimization analysis. Another noteworthy point to observe in Fig. 9b is that the ($\dot{Q}_{in}$) and the ($P_{el,motor}$) seems to have an inverse proportional variation. This occurs reasonably considering that the lower the input thermal power to the cycle, the higher the work demand in the compressor for achieving the same useful output of 1000 kW_{th}. As Fig. 9c indicates, the outlet preheated air temperature seems to follow the same variation profile as the inlet one, considering that the output thermal power is assumed to be constant, something that results, also, in the maintenance of a constant temperature difference of the preheated air stream. The fluctuation of the exhaust gases outlet temperature appears to be negligible during the examined period, with the mean value being around 70 °C. Fig. 9d shows that both the turbine and the compressor's pressure ratio fluctuation are analogous to the inlet preheated air temperature variation. Another aspect to notice is that the pressure ratio of the compressor exceeds the respective pressure ratio of the turbine, something that occurs due to the pressure drop effect, which is added in the closed circuit from the heat exchanger devices. As a general observation, several sharp peaks and valley points can be identified in all diagrams presented in Fig. 9. The most pronounced of these occur within the first 84 h of the examined time period, appearing with a periodicity of approximately 18–23 h. This behaviour is primarily attributed to the preheated air inlet temperature profile, shown in Fig. 9c, which constitutes the main input variable of the present dynamic analysis. As illustrated in the figure, the inlet air temperature exhibits distinct peak values that coincide with the times at which the corresponding peaks and valleys appear in the other diagrams of Fig. 9. These temperature peaks are associated with the daily production schedule of the kiln. During operation, the kiln remains empty for short periods to allow product sorting and evaluation, while it is intentionally kept running rather than shut down in order to avoid thermal inertia losses that would otherwise lead to significantly higher power consumption during restart. This short no-load operating period causes a noticeable increase in the air temperature levels inside the kiln. As a result, the elevated preheated air inlet temperature directly affects the operating conditions of the examined high-temperature heat pump (HTHP), leading to the appearance of the observed minimum and maximum values across the diagrams in Fig. 9.

Environmental analysis

Following the thermodynamic calculations and the determination of the optimum HTHP heat integration configuration within the existing process, a further evaluation of the dynamic analysis results was performed to quantify the benefits of integrating the HTHP system into the examined industrial process and to assess the associated environmental impact. To this end, the dynamic results were extrapolated to full-year operation, enabling the calculation of annual values for all relevant parameters, including the useful heat output of the HTHE, the heat input from the LTHE, and other key performance indicators. The HTHP was assumed to operate for 50 weeks per year (8,400 h) by repeating the representative weekly operating profile of 168 h across the 50-week period.

In the present annual analysis, great emphasis is given on the energy savings resulting from NG consumption reduction due to the partial electrification (~10%) of the process ensured by the utilization of the HTHP. The environmental impact of the proposed integration is also evaluated, considering the CO_2 emissions as a main criterion. The total annual useful energy output coming from HTHP is first calculated and found to be 8400 MWh/year, considering that the thermal power output is steady and equal to 1 MW_{th}. This useful heat is assumed to be obtained in the kiln combustion zone in the form of high-temperature preheated air, leading to the reduction of the NG heat demand and, as a result, to lower NG consumption. Then the annual electrical energy consumption of the HTHP is calculated. The primary energy consumption was determined for both the NG and the HTHP case, considering primary energy factors of 1.05 and 1.91, respectively [39,40]. The CO_2 emissions expected from the specific natural gas saved portion are determined and compared directly to the respective emissions arising from the HTHP electrical energy consumption. The emission factors which are utilized for the aforementioned calculations are 0.196 $t_{CO2\text{-}eq}$/MWh for the natural gas [41] and 0.232 $t_{CO2\text{-}eq}$/MWh for the electrical energy [42], while the efficiency of the natural gas burners is taken equal to 80% [43,44]. The electricity and natural gas costs were derived from the industry's billing records, with values of 100.7 €/MWh and 43.5 €/MWh, respectively, while the carbon emission cost was assumed to be 80 €/t [45]. The comparison between the baseline case (NG burners) and the retrofitted one (NG burners + HTHP) was performed considering as the comparison basis the total energy consumption of the production line, which includes the natural gas burned in the combustion zone and the electricity consumed for the operation of the HTHP. The annual dynamic analysis results are presented comprehensively in Table 3, including the primary energy and the emissions calculations, as well as the financial evaluation of the two scenarios.

Despite the fact that the CO_2 emissions factor for electricity consumption is 18.4% higher than that of natural gas, the total emissions appear to be reduced with the integration of the HTHP. Particularly, the installation of the HTHP results in a 5.44% reduction in CO_2 emissions, clearly demonstrating the added environmental benefit of the proposed configuration and the upgrade of the roof tiles production line. Another important finding is that the proposed integration leads to a remarkable 13.04% NG consumption reduction, further indicating the positive environmental impact of the present integration. The energy saving in primary energy terms is calculated to be 1154 MWh_{PE}/year (1.36%).

In the financial evaluation analysis, it was observed that the total cost is found to be approximately the same in both the baseline and the retrofitted cases, with a negligible difference of 0.11% to be observed. Therefore, the integration of the HTHP provides both lower carbon emissions and higher primary energy savings, while maintaining total operating costs comparable to the baseline configuration. It is worth mentioning that when the HTHP useful output is considered to be greater than 1 MW_{th}, lower CO_2 emissions are expected to be achieved with a slight penalty in the total operating cost. For instance, if the HTHP is assumed to produce 2 MW_{th} useful thermal power, then it is predicted that the CO_2 emissions decreased by approximately 9.8% compared to the baseline case, with the total operating cost to barely exceed the baseline scenario's by less than 2%. This prediction was conducted through the utilization and further treatment of the useful output effect analysis results presented in section 3.3, considering a mean preheated air inlet temperature of 150 °C. As far as the capital expenditure (CAPEX) is concerned, it should be mentioned that the Reverse Brayton HTHP is still an under-development technology and thus it is accompanied by relatively high manufacturing costs, which results in a payback period of over 30 years, something that introduces sustainability limitations in potential integration without subsidy. However, the potential of this technology should not be ignored, considering that possible mass production could ensure lower capital costs and enhance the integration sustainability.

Table 3
Environmental and financial impact evaluation of the examined cases.

Analysis parameters	Baseline	Retrofitted	Difference
NG consumption (MWh_{NG}/year)	80,500	70,000	13.04%
Electricity consumption (MWh_{el}/year)	0	5168	–
NG Primary Energy consumption (MWh_{PE}/year)	84,525	73,500	13.04%
Electricity Primary Energy consumption (MWh_{PE}/year)	0	9871	–
Total Primary Energy consumption (MWh_{PE}/year)	84,525	83,371	1.36%
NG CO_2 emissions (t_{CO2_eq}/year)	15,778	13,720	13.04%
Electricity CO_2 emissions (t_{CO2_eq}/year)	0	1199	–
Total CO_2 emissions (t_{CO2_eq}/year)	15,778	14,919	5.44%
CO_2 cost (€/year)	1,262,240	1,193,523	5.44%
NG cost (€/year)	3,501,750	3,045,000	13.04%
Electricity cost (€/year)	0	520,444	–
Total cost (€/year)	4,763,990	4,758,967	0.11%

Discussion

Scalability to other industrial sectors: Constraints and requirements

Although the current study presents a single case in the KEBE industry in the ceramic rooftiles sector, the Reverse Brayton HTHP technology could be a promising solution for implementation in various industrial applications in different ceramic plants or other sectors (cement, glass, rubber, pulp & paper, sewage, etc.), ensuring efficient utilization of the waste heat in several heating processes. However, the integration of a Reverse Brayton HTHP in a specific industrial environment is accompanied by various constraints and adaptation requirements that should be considered for evaluating the integration potential properly in each case.

Generally, waste heat recovery opportunities normally appear in several industrial processes along the production line (drying, preheating, cooling, etc.) in all the aforementioned sectors, with differentiations in the outlet temperature of the heat source medium (e.g., flue gases, vapor, air), considering that different raw materials are being processed in each case. Indicated ranges for the aforementioned outlet temperature are approximately 250–380 °C for cement production (flue gases/cement preheating) [46,47], 100–150 °C for pulp and paper industry (exhaust vapor/pulp drying) and 90–100 °C for sewage industry (exhaust air/sludge drying) [48].

In any case, it is important to investigate any possible constraint that accompanies each industrial process. These constraints could correspond to process integration, flue gas composition, thermodynamic and economic limitations. In the cement industry, the flue gases carry high concentrations of dust and abrasive particles (e.g., raw meal, clinker dust, etc.). These substances could rapidly erode the heat exchanger's active surfaces, leading to a significant degradation in the thermal effectiveness of the heat exchangers and thus of the system's performance, while increasing at the same time the need for maintenance, which in turn introduces extra costs and complexity in the production procedure. In that case, materials or coatings with high abrasion resistance could be selected in combination with the implementation of robust cleaning strategies (periodic blowdowns, etc.) to ensure performance sustainability, by increasing significantly the manufacturing costs. In the case of the glass industry, waste gas streams often contain vapors and compounds from the glass melt, which could rapidly accelerate heat exchanger deterioration, unless high alloys or anti-corrosive coated surfaces are used. In the pulp and paper industry, excessive moisture in the stream could promote fouling and corrosion of the HTHP's heat exchangers. As far as the rubber industry is concerned, exhaust gases usually contain volatile and organic compounds (VOCs), which, in combination with moisture, set severe safety and compatibility challenges for heat exchangers' materials, which should be considered. To mitigate this, pretreatment of the exhaust gas (e.g., catalytic oxidation and condensation removal) is strongly recommended.

It is important to mention that, considering the relatively low heat source temperatures (<150 °C) in industries such as pulp and paper, textile and sewage, possible integration of Reverse Brayton HTHP units should be examined carefully since a less efficient operation is expected. For encountering that issue, great emphasis should be given to the optimization of HTHP, considering the variation of several different operating parameters (multi-objective optimization) to ensure a sustainable high-performance operation.

Future work

In summary, the investigated integration appears to be a promising proposal for achieving significant energy savings and CO_2 emissions reduction in the ceramics sector via the utilization of low-temperature waste heat using a novel HTHP set-up. Future work could involve examining alternative Reverse Brayton HTHP configurations (e.g., cascade, reheating, etc.) to achieve even higher useful power output. Additionally, exploring Reverse Brayton cycles with different working mediums represents a promising direction for broadening the operating range of HTHP systems, thereby enabling greater energy savings and further reductions in carbon emissions. It is important to mention that a detailed economic analysis considering the Capital Expenditure (CAPEX) and the maintenance costs would be beneficial for evaluating in depth the economic viability of a similar integration to the proposed HTHP integration in an industrial environment. This would ensure a proper decision making procedure as regards the determination of the final specifications and the main design characteristics of critical components (turbocharger unit, heat exchangers, motor etc.), the selection of the suitable suppliers and the proper organization of all the necessary procedures which should be followed during the design and the optimization process of such technologies as well as during the manufacturing, commissioning and integration of them to existing industrial sites. Moreover, a detailed investigation of the useful heat output variation effect considering dynamic operating conditions would be very useful for possible future investigation, including evaluation of the respective annual savings and environmental impact. Finally, performing a detailed exergy destruction analysis for each HTHP component would be a valuable extension of this work. Such an analysis would allow for an in-depth evaluation of the thermodynamic performance and irreversibility sources within the compressor, turbine, and heat exchangers. Specifically, this analysis should involve a detailed design investigation regarding the heat exchanger devices of the HTHP, giving great emphasis to the HTHE and the LTHE geometries, aiming for the optimal matching between the temperature profiles of the primary and secondary flow streams in each heat exchanger case for ensuring the minimization of the exergy destruction. Additionally, it would provide insights into the influence of design parameters on component-level efficiency and enable further optimization targeted at improving the performance of each HTHP component.

Conclusions

The present work investigated the integration of an HTHP system in the KEBE ceramics industry in northern Greece, with the aim of reducing natural gas consumption in the kiln of the roof tiles production line. The system operation was first optimized and then dynamically analyzed using actual operational data to assess its potential for energy efficiency improvement, environmental impact mitigation, and overall sustainability. Model validation confirmed the accuracy of the developed MATLAB model, showing deviations below 0.60% compared to the independent EBSILON model under steady state and selected operating conditions. Following the verification of the in-house MATLAB model, an optimization analysis was performed, revealing the existence of an optimal working fluid mass flow rate at which the COP, exergy efficiency, and inlet thermal power were simultaneously maximized for each examined preheated air inlet temperature within the range 100–200 °C. The results indicated that both the COP and the inlet thermal power increased as the inlet air temperature decreased, while the exergy efficiency followed the opposite trend, in line with thermodynamic expectations. A linear negative correlation was observed between the optimal mass flow rate and the inlet preheated air temperature, and an empirical correlation describing this dependency was derived. The dynamic simulation of the integrated HTHP demonstrated that the system achieved a COP ranging from 1.50 to 1.75, which is considered satisfactory given the high-temperature operation of the kiln. Annual performance analysis further demonstrated the environmental benefits of the system: CO_2 emissions were reduced by 5.44%, accompanied by a 13.04% and 1.36% reduction in NG and in primary energy consumption, respectively. The mean COP over the annual operation was calculated as 1.63, indicating consistent performance throughout the year. Overall, these results highlight the substantial potential of HTHP integration in high-temperature industrial processes, both in terms of energy savings and environmental impact reduction. The study provides a quantitative basis for further deployment of HTHPs in the ceramics industry and similar sectors.

CRediT authorship contribution statement

Dimitrios N. Korres: Writing – original draft, Validation, Software, Methodology, Investigation, Data curation, Conceptualization. **Evangelos Bellos:** Writing – original draft, Methodology, Investigation, Data curation, Conceptualization. **Nikolaos Nikolopoulos:** Writing – original draft, Supervision, Methodology, Conceptualization. **Varshil Dalal:** Writing – original draft, Validation, Software. **Panagiotis Stathopoulos:** Writing – original draft, Supervision. **Apostolos Gkountas:** Writing – original draft, Methodology, Investigation. **Pantelis Bakalis:** Writing – original draft, Project administration. **Ilias K. Tragazikis:** Writing – original draft, Resources. **Agis Kothalis:** Writing – original draft, Resources.

Declaration of competing interest

The authors declare that they have no known competing financial interests or personal relationships that could have appeared to influence the work reported in this paper.

Acknowledgments

This work has been carried out in the framework of the European Union's Horizon Europe programme under grant agreement No 101178624 (Energy Efficiency and Electrification Technologies for Heat Flow Optimization in Process Industries – EEETHOS).

Appendix A

Investigation of the system performance for different specific heat capacity values of the flue gases

In this Appendix, a detailed analysis is performed to evaluate the impact of the modelling assumption adopted in the present study, where the flue gas properties are approximated as those of air, on the performance of the examined high-temperature heat pump (HTHP). The main thermodynamic property affecting the modelling results is the specific heat capacity of the flue gas, as it directly influences the heat transfer calculations in the Low-Temperature Heat Exchanger (LTHE). Therefore, the analysis focuses primarily on the sensitivity of the results to this parameter.

For the approximation of real flue gases, the specific heat capacity at 90 °C was assumed equal to 1.05 kJ kg^{-1} K^{-1} according to the study [49]. This value corresponds to flue gas generated from natural gas combustion with excess air, which closely represents typical industrial operating conditions. Fig. A1 compares the air assumption with the real flue gas approximation in terms of the coefficient of performance (COP) and the compressor pressure ratio (PR_C). The calculations were carried out assuming a preheated air inlet temperature of 150 °C.

As depicted in Fig. A1, the assumption of treating the flue gases main properties and particularly the specific heat capacity as equal to that of air, provides a sufficiently accurate approximation of the real flue gas properties, as only minor deviations (<1%) are observed in both the COP and PR_C curves. More specifically, the maximum deviation in COP does not exceed 0.76%, while the corresponding deviation in PR_C remains below 0.48%. Therefore, approximating the flue gases as air can be considered a safe and reasonable modelling approach within the framework of the present study.

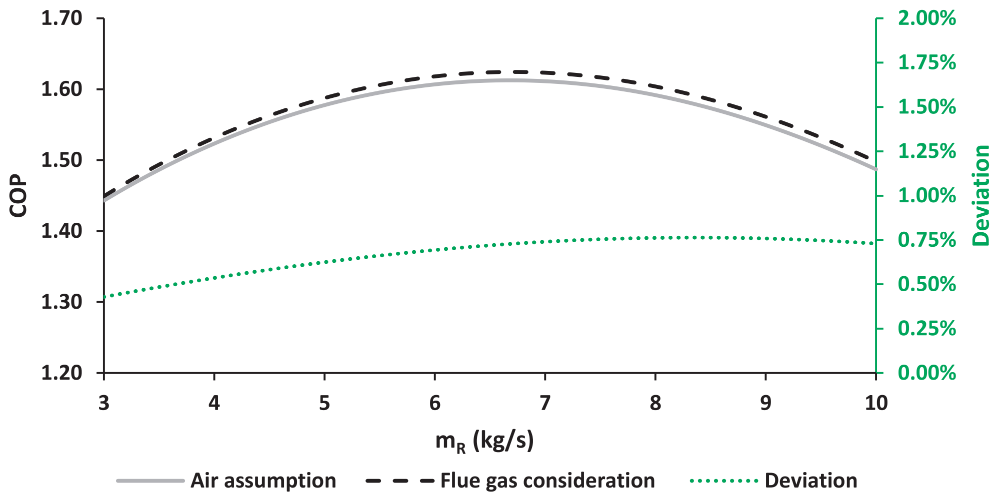

(a)

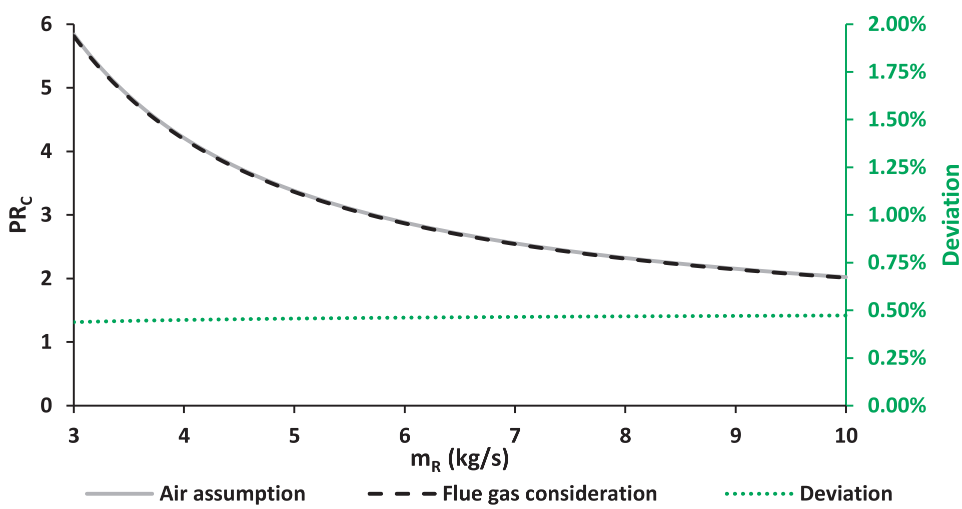

(b)

Fig. A1. Air assumption versus real flue gases approximation: (a) COP and (b) PR_C curves for $T_{PA,in}$ = 150 °C.

Data availability

The data that has been used is confidential.

References

[1] Abbasi MH, Abdullah B, Ahmad MW, Rostami A, Cullen J. Heat transition in the European building sector: overview of the heat decarbonisation practices through heat pump technology. Sustainable Energy Technol Assess 2021;48:101630. https://doi.org/10.1016/j.seta.2021.101630.

[2] Huang Y, Li G, Tang X, Huang K, Zhao W, Zhang J. Thermodynamic analysis of a modified cascade high temperature heat pump with zeotropic mixtures for heating

production up to 200 °C. Energ Conver Manage 2025;324:119307. https://doi.org/10.1016/j.enconman.2024.119307.
[3] Gadagkar D, Hoess AJ, Ziviani D, Barta RB. Modeling of high-temperature heat pump cycles for industrial applications using moving boundary heat exchangers and advanced cycle architectures. Applied Thermal Engineering. 2025; [published online ahead of print]. doi: https://doi.org/10.1016/j.applthermaleng.2025.129039Arpagaus C, Bless F, Uhlmann M, Schiffmann J, Bertsch SS. High temperature heat pumps: Market overview, state of the art, research status, refrigerants, and application potentials. Energy. 2018;152:985-1010. doi: https://doi.org/10.1016/j.energy.2018.03.166.
[4] Furszyfer Del Rio DD, Sovacool BK, Foley AM, et al. Decarbonizing the ceramics industry: a systematic and critical review of policy options, developments and sociotechnical systems. Renew Sustain Energy Rev 2022;157:112081. https://doi.org/10.1016/j.rser.2022.112081.
[5] Branchini L, De Pascale A, Ottaviano S, Poletto C. Application of high-temperature heat pumps in the ceramic tiles manufacturing sector for waste heat harnessing. Appl Therm Eng 2025;274:126694. https://doi.org/10.1016/j.applthermaleng.2025.126694.
[6] Manrique R, Vasquez D, Vallejo G, Chejne F, Amell AA, Herrera B. Analysis of barriers to the implementation of energy efficiency actions in the production of ceramics in Colombia. Energy 2018;143:575–84. https://doi.org/10.1016/j.energy.2017.11.023.
[7] Valdés CF, Chejne F, Marrugo G, et al. Co-gasification of sub-bituminous coal with palm kernel shell in fluidized bed coupled to a ceramic industry process. Appl Therm Eng 2016;107:1201–9. https://doi.org/10.1016/j.applthermaleng.2016.07.086.
[8] Ahmed MM, Kassim A, Ragab A, et al. Enhanced strength, durability, and thermal shock resistance of clay roof tiles substituted with ferrosilicon slag. J King Saud Univers Sci 2023;35(5):102855. https://doi.org/10.1016/j.jksus.2023.102855.
[9] Amin SK, Ashmawy NMF, Abadir MF. The use of tannery waste in the preparation of clay roof tiles. Constr Build Mater 2022;325:126393. https://doi.org/10.1016/j.conbuildmat.2022.126393.
[10] Martínez-Martínez S, Pérez-Villarejo L, Garzón E, Sánchez-Soto PJ. Influence of firing temperature on the ceramic properties of illite-chlorite-calcitic clays. Ceram Int 2023;49(15):24541–57. https://doi.org/10.1016/j.ceramint.2022.11.077.
[11] Obrist MD, Kannan R, McKenna R, Schmidt TJ, Kober T. High-temperature heat pumps in climate pathways for selected industry sectors in Switzerland. Energy Policy 2023;173:113383. https://doi.org/10.1016/j.enpol.2022.113383.
[12] Ibanez-Flores V, Bovea MD, Azapagic A. Assessing the sustainability of best Available techniques (BAT): methodology and application in the ceramic tiles industry. J Clean Prod 2013;51:162–76. https://doi.org/10.1016/j.jclepro.2013.01.020.
[13] Department for Business, Energy & Industrial Strategy (BEIS). Ceramic Sector: Joint Industry - Government Industrial Decarbonization and Energy Efficiency Roadmap Action Plan. Published October 2017. Accessed [19/11/2025]. https://www.gov.uk/government/publications/industrial-decarbonisation-and-energy-efficiency-roadmaps-action-plans.
[14] Jouhara H, Zabnieńska-Góra A, Delpech B, Olabi V, El Samad T, Sayma A. High-temperature heat pumps: fundamentals, modelling approaches and applications. Energy 2024;303:131882. https://doi.org/10.1016/j.energy.2024.131882.
[15] Wang R, Yan H, Wu D, Jiang J, Dong Y. High temperature heat pumps for industrial heating processes using water as refrigerant. Energy 2024;313:133847. https://doi.org/10.1016/j.energy.2024.133847.
[16] Deng N, Jing X, Cai R, et al. Molecular simulation and experimental investigation for thermodynamic properties of new refrigerant NBY-1 for high temperature heat pump. Energ Conver Manage 2019;179:339–48. https://doi.org/10.1016/j.enconman.2018.10.076.
[17] Yu X, Zhang Y, Deng N, Chen C, Ma L, Dong L, et al. Experimental performance of high temperature heat pump with near-azeotropic refrigerant mixture. Energy Build 2014;78:43–9. https://doi.org/10.1016/j.enbuild.2014.04.011.
[18] Dong Y, Yan H, Wang R. Significant thermal upgrade via cascade high temperature heat pump with low GWP working fluids. Renew Sustain Energy Rev 2024;190:114072. https://doi.org/10.1016/j.rser.2023.114072.
[19] Arpagaus C, Bless F, Uhlmann M, Schiffmann J, Bertsch SS. High temperature heat pumps: market overview, state of the art, research status, refrigerants, and application potentials. Energy 2018;152:985–1010. https://doi.org/10.1016/j.energy.2018.03.166.
[20] Tran AP, Stathopoulos P. Dynamic simulation and experimental validation of a high-temperature Brayton heat pump. Appl Therm Eng 2025;274:126536. https://doi.org/10.1016/j.applthermaleng.2025.126536.
[21] Kabat N, Jende E, Nicke E, Stathopoulos P. Investigation on process architectures for high-temperature heat pumps based on a reversed Brayton cycle. In: Proceedings of the ASME Turbo Expo 2023: Turbomachinery Technical Conference and Exposition; June 26-30, 2023; Boston, Massachusetts, USA. GT2023-102497. doi: https://doi.org/10.1115/GT2023-10249.
[22] Kabat N, Jende E, Yücel FC, Stathopoulos P. Thermodynamic analysis of a novel high-temperature heat pump cycle with inter cooled compression and reheated expansion based on the reversed Brayton cycle. International Journal of Sustainable Energy. Published online June 26, 2025. doi: https://doi.org/10.1080/14786451.2025.2515452.
[23] Yücel FC, Oehler J, Kriese M, et al. Design, commissioning and closed-loop operation of a high-temperature Brayton heat pump — CoBra. Appl Therm Eng 2025;279:127947. https://doi.org/10.1016/j.applthermaleng.2025.127947.
[24] Tzouganakis P, Bellos E, Rakopoulos D, Skembris A, Rogkas N. Thermodynamic analysis of a solar-fed heat upgrade system using the reverse air brayton cycle. Renew Energy 2025;238:121975. https://doi.org/10.1016/j.renene.2024.121975.
[25] Tzouganakis P, Rakopoulos D, Bellos E, Skembris A, Rogkas N, Jende E, Dalal V. Optimized operation of a combined solar and waste heat driven high temperature heat pump for a food industry. Paper presented at: 38th International Conference on Efficiency, Cost, Optimization, Simulation and Environmental Impact of Energy Systems; June 29-July 4, 2025; Paris, France.
[26] Pettinari M, Frate GF, Tran AP, Oehler J, Stathopoulos P, Ferrari L. Transient analysis and control of a Brayton heat pump during start-up. Paper presented at: Proceedings of ECOS 2023 - The 36th International Conference on Efficiency, Cost, Optimization, Simulation and Environmental Impact of Energy Systems; June 25-30, 2023; Las Palmas de Gran Canaria, Spain.
[27] Gollasch J, Agelidou E, Henke M, Stathopoulos P. Conceptual study of thermally coupled micro gas turbines and high temperature heat pumps for trigeneration. Paper presented at: ASME Turbo Expo 2022: Turbomachinery Technical Conference and Exposition; June 13-17, 2022; Rotterdam, Netherlands. GT2022-81959. doi: https://doi.org/10.1115/GT2022-81959.
[28] KEBE SA ceramics industry. Accessed [19.11.2025]. https://www.kebe-sa.gr/en/.
[29] EEETHOS Project: Energy Efficiency and Electrification Technologies for Heat Flow Optimization in Process Industries. Accessed [19.11.2025]. https://eeethos-project.eu/.
[30] Bujak J, Sitarz P, Bujak K, Majkowski S, Pasela R. Estimation complete combustion coefficient in rotary kilns. Energies 2022;15:1143. https://doi.org/10.3390/en15031143.
[31] Korres D, Tzivanidis C, Koronaki IP, Nitsas MT. Experimental, numerical and analytical investigation of a U-type evacuated tube collectors' array. Renew Energy 2019;135:218–31. https://doi.org/10.1016/j.renene.2018.12.003.
[32] The MathWorks Inc, Optimization Toolbox Version: 9.4 (R2022b), The MathWorks Inc, Natick, Massachusetts, 2022.
[33] UNILAB. Coils User Manual. Scribd. Published 2023. Accessed [19.11.2025]. https://www.scribd.com/document/866804912/UNILAB-Coils-User-Manual.
[34] Bell I. MATLAB Interface for REFPROP and CoolProp. MATLAB Central File Exchange. Updated October 18, 2024. Accessed [19.11.2025]. https://www.mathworks.com/matlabcentral/fileexchange/180324-matlab-interface-for-refprop-and-coolprop.
[35] Iqony Solutions GmbH. EBSILON®Professional: Release Notes (English), Release 17.0. Zwingenberg, Germany: Iqony Solutions GmbH 2024.
[36] Kabat N, Oehler J, Stathopoulos P. Experimental Exergy Analysis of a High-Temperature Brayton Heat Pump. In: 70th ASME Turbo Expo 2025: Turbomachinery Technical Conference and Exposition, GT 2025, 2025-06-16 - 2025-06-20, Memphis, Tennessee, USA. doi: http://doi.org/10.1115/GT2025-153648, ISBN 978-079188887-2.
[37] Variable speed drive air compressors. Atlas Copco AB. Published 2026. Accessed [03.04.2026]. https://www.atlascopco.com/en-gr/compressors/wiki/compressed-air-articles/what-is-a-vsd-compressor.
[38] Durrheim C. Risk management: Advancements in variable speed drive technology for reducing operational risk. Australian and New Zealand Grapegrower and Winemaker, 2019;669;64-65. Accessed [03.04.2026]. Available [online]: https://search.informit.org/doi/abs/10.3316/ielapa.925281791090621.
[39] Federation of European Heating, Ventilation and Air Conditioning Associations (REHVA). Technical guidance for EPBD implementation: Task Force March 18th, 2024. REHVA Journal. Published 2024. Accessed [19.11.2025]. https://www.rehva.eu/rehva-journal/chapter/technical-guidance-for-epbd-implementation-task-force-march-18th-2024.
[40] Support to primary energy factors review (PEF) – Final report, Publications Office of the European Union, 2023, Accessed [19.11.2025], https://data.europa.eu/doi/10.2833/404077.
[41] Technical Chamber of Greece (TEE). *TOTEE 20701-1: 2017: Energy Performance of Buildings Directive - National Calculation Methodology.* Scribd. Published 2017. Accessed [19.11.2025]. https://www.scribd.com/document/373181643/TOTEE-20701-1-2017-TEE-1st-Edition.
[42] Hellenic Republic - Ministry of Environment and Energy. Energy Mix 2024. DAPEEP. Published June 2025. Accessed [19.11.2025]. https://www.dapeep.gr/wp-content/uploads/2025/06/ΕΝΕΡΓΕΙΑΚΟ-ΜΕΙΓΜΑ-2024-2.pdf.
[43] Honeywell. Honeywell Burner Models. Scribd. Published online 2022. Accessed [19.11.2025]. https://www.scribd.com/document/677596954/Honeywell-Burner-Models.
[44] Mickey SR, Schönfelder MG, Wünning JG. Efficient gas heating of industrial furnaces. Thermal Processing. Published September 1, 2018. Accessed [19.11.2025]. https://thermalprocessing.com/efficient-gas-heating-of-industrial-furnaces/.
[45] European Commission. Trends in carbon intensity and the macroeconomic role of the EU Emissions Trading System. Economy & Finance. Published November 17, 2025. Accessed [20.11.2025]. https://economy-finance.ec.europa.eu/recent-trends-carbon-intensity-eu-economy-and-macroeconomic-role-carbon-pricing-through-eu-emission_en.
[46] Mungyeko Bisulandu B-J-R, Ilinca A, Tsimba MM, Mbozi ML. Thermodynamic performance of a cogeneration plant driven by waste heat from cement kilns exhaust gases. Energies 2023;16(2460). https://doi.org/10.3390/en16052460.
[47] Scheuch GmbH. Selective Catalytic Reduction (SCR). Published 2013. Accessed March 6, 2026. https://scheuch-industrial-solutions.com/en/download/scr/.
[48] IEA HPT. Annex 58: High-Temperature Heat Pumps - Task 1: Technologies Task Report. Published 2023. Accessed March 6, 2026. https://heatpumpingtechnologies.org/content/uploads/sites/70/2023/09/annex-58-task-1-technologies-task-report.pdf.
[49] Coskun C, Oktay Z, Ilten N. A new approach for simplifying the calculation of flue gas specific heat and specific exergy value depending on fuel composition. Energy 2009;34:1898–902. https://doi.org/10.1016/j.energy.2009.07.040.